AN INVESTIGATION OF THE NUCLEAR LIPID ASSOCIATED PROMYELOCYTIC LEUKEMIA (PML) STRUCTURES (LAPS) PROTEOME USING BIOTIN PROXIMITY LABELLING

by

Jordan Spencer Thompson

Submitted in partial fulfilment of the requirements

for the degree of Master of Science

at

Dalhousie University

Halifax, Nova Scotia

August 2022

DEDICATION PAGE

Approximately a long time ago there was nothing for a debatable amount of time. Aristotle would argue it was infinite since there was no one around to check the time, while Einstein would say that the distinction is meaningless due to the convergence of spacetime. Then suddenly, things got hot really fast and there were some elementary particles. Fast forward and there is a planet with these elementary particles managing to form self-replicating biomolecules that have some genetic information. A few billion years after that and a few endosymbiosis events later, some genetic information comes together forming a bundle of cell. Finally, precisely 24 years later these bundles of cells completed his thesis on the study of cells and biomolecules. Looking at how things started, who would have guessed this outcome.

I dedicate this thesis to all the cells and biomolecules that worked together to make this happen.

TABLE OF CONTENTS

LIST OF FIGURES

ABSTRACT

Fatty acids are stored in triacyl glycerides or cholesterol esters in lipid droplets (LDs). While most LDs are cytoplasmic, there are also nuclear lipid droplets (nLDs) that associate with promyelocytic leukemia (PML) called Lipid Associated PML Structures (LAPS). The protein composition of LAPS is distinct from PML nuclear bodies but the complete LAPS proteome has not been characterized. To address this, APEX2 proximity labelling was used to identify proteins that interact with LAPS. Using this approach, protein mitogen-activated protein kinase-activated protein kinase 2 (MK2) was identified as a high confidence interactor. Immunofluorescence confocal microscopy showed that two MK2 isoforms associated with LAPS. When the kinase activity of MK2 was inhibited, there was an increase in LAPS/cell. While oleate treatment had an inconsequential effect on the p38 signaling cascade, this pathway was severely dysregulation in PML-deficient U2OS cells. In conclusion, MK2 was identified and validated as a LAPS-interacting kinase.

LIST OF ABBREVIATIONS USED

AGPAT	1-acylglycerol 3-phosphate acyltransferases
ATGL	adipose triglyceride
APB	ALT associated PML bodies
ALT	alternative lengthening of telomeres
ApoB	apolipoprotein B100
AREs	AU-rich elements
CE	cholesterol esters
CEPT	choline/ethanolamine phosphotransferase
CCTα	CTP: phosphocholine cytidyltransferase
cLDs	cytoplasmic lipid droplets
DAXX	death domain-associated protein 6
DAG	diacyl glycerol
DGAT	diacylglycerol acyltransferase
DMSO	dimethyl sulfoxide
DTT	dithiothreitol
DMEM	Dulbecco's modified eagle medium
eLD	nucleoplasmic reticum-lumeninal lipid droplet
ER	endoplasmic reticulum
ESCRT	endosomal sorting complexes required for transport
EDTA	Ethylenediaminetetraacetic acid
FBS	fetal bovine serum
GPAT	glycerol 3-phosphate acyltransferase
HSP27	heat shock protein 27
HCV	hepatitis C virus
HPLC	high-performance liquid chromatography
HSL	hormone sensitive lipase
HGPS	Hutchinson–Gilford progeria syndrome
INM	inner nuclear membrane
KO	knock out
LFQ	label-free-quantification
LBR	lamin B1 receptor
LAPS	lipid associated PML structures
LDAF1	lipid droplet assembly factor 1
LD	lipid droplets
LC-MS/MS	liquid Chromatography with tandem mass spectrometry
mTORC1	mammalian target of rapamycin complex 1

MK2	mitogen-activated protein kinase-activated protein kinase 2
MVB	multivesicular bodies
NAFLD	non-alcoholic fatty liver disease
NASH	non-alcoholic steatohepatitis
nLD	nuclear lipid droplet
NLS	nuclear localization signal
PASEF	parallel accumulation-serial fragmentation
PNPLA3	patatin like phospholipase domain-containing protein 3
PPARα	peroxisome proliferator-activated receptor α
PF	PF-3644022
PMSF	phenylmethanesulfonylfluoride
PC	phosphatidylcholine
PBS.	phosphate buffed saline
PLIN2	perilipin 2
PGC-1α	PPAR gamma coactivator 1
PML	promyelocytic leukemia
RIPK1	receptor-interacting serine/threonine-protein kinase 1
RBCC	RING finger/ B box/ coiled coil
SB	SB-203580
SUMO	small ubiquitin like modifier
SDS	sodium dodecyl sulfate
SREPB	sterol regulatory element-binding protein
SIM	SUMO interacting motif
SRRF	super resolution radial fluctuation
TAG	triacyl glyceride
TFA	trifluoroacetic acid
TRIM	tripartite motif
TNF	tumor necrosis factor
VLDL	very low-density lipoprotein

ACKNOWLEDGEMENTS

There are many people who without their help, I would not be able to complete this research. I would like to thank my committee members Graham Dellaire and Thomas Pulinilkunnil for their continued support and feedback. I also would like to thank both Jayme Salsman from the Dellaire lab, and Brianne Lindsay from the CMDI for their aid and expertise with microscopy. There are also my collaborators in the Boisvert lab from Université Sherbrooke who performed the LC-MS/MS analysis.

I would like to acknowledge the members of the Ridgway lab team. This is of course led by my supervisor Neale Ridgway who took in a stray undergraduate, and I guess decided to keep him. His guidance, knowledge, and patience have made this odyssey possible. Rob Douglas helped with his cell culture expertise, and Brenda O'Brien with her administrative prowess. I would like to thank my lab mates Gabriel Dorighello, and Katie Halliday. The former for always bringing a smile to the lab, and the latter for making me realize at least my problems aren't as bad as others. Lastly, there are the other two members of the Ridgway Roommate Triumvirate: Mike McPhee and Jason Foster. They served as great lab mentors and as even better friends.

Lastly, there are my parents Derrick and Kelli for whom without their gametes, this would not be possible. Their love and support over these long years have borne fruit at last. You both have served as role models for my endeavors with your motto: "Work hard, Play hard".

Chapter 1: Introduction

1.1 Research Objectives

My MSc research had two objectives: 1) to utilize APEX2 proximity labelling to determine the protein interactome of promyelocytic leukemia (PML) and lipid associated PML structures (LAPS) and 2) to functionally characterize the high confidence protein interactors determined by the APEX2 proximity labelling.

For the first objective, I constructed plasmids expressing an APEX2 fusion protein with PML isoforms I and II, as well as a control plasmid that expressed APEX2 modified with a nuclear localization signal (NLS). I transfected these plasmids into U2OS cells, induced nuclear lipid droplet (nLD) formation with oleate and labeled nearby proteins with APEX2 by providing cells with H_2O_2 and biotin phenol. Using this approach, I generated a list of proteins that associate with PML-I and PML-II in the presence and absence of oleate-induced LAPS.

For the second objective, I focussed on a high confidence PML and LAPS interactor, mitogen-activated protein kinase-activated protein kinase 2 (MK2). I investigated how MK2 associates with PML isoforms, as well as how MK2 phosphorylation through the p38 kinase pathway affects LAPS formation using both phosphorylation inhibitors as well as siRNA knockdown.

This thesis will begin with a review of nuclear lipid droplets (nLDs), their composition, formation, and what makes them unique from their cytoplasmic counterparts. This will be followed by a review of the PML protein before talking about

how these two topics intersect with LAPS. Lastly, I will discuss how proximity labelling is used to identify high confidence interactors in biomolecular protein complexes.

1.2 Lipid Droplet Structure

Lipid droplets (LDs) are lipid storage organelles found in all eukaryotes and some prokaryotes. They consist of a phospholipid monolayer that surrounds a neutral lipid core [1]. The neutral lipid core can contain triacyl glycerides (TAG), cholesterol esters (CE) and retinyl esters [2]. LDs are dynamic organelles that expand under nutrient starvation or lipid overload conditions and are catabolized through two different mechanisms: lipolysis and lipophagy. Lipolysis is the major mechanism of lipid droplet degradation. This process is initiated by protein kinase A phosphorylating PLIN1 leading to increased access to the LD core for lipases such as adipose triglyceride lipase (ATGL; a.k.a. PNPLA2) or hormone sensitive lipase (HSL) which hydrolyse TAG and DAG molecules [3, 4]. The process of lipophagy is a type of macroautophagy. LC3-II positive membranes encircle LDs and fuse with lysosome to form the autolysosome which degrades the lipids [5, 6].

LDs have numerous interactions with other organelles such as the endoplasmic reticulum (ER), mitochondria, peroxisomes, and lysosomes. The ER is the site of cytoplasmic LD (cLD) formation and lipid and protein transfer between the two organelles occurs at these junctions [7, 8]. The interactions between LDs and mitochondria occur mostly to facilitate the steady release of fatty acids for β-oxidation [9]. In plants and yeasts, where peroxisomes are the site of β-oxidation, the peroxisome-

LD interaction has a similar role to that of the mitochondria in animal cells [10]. The role is altered in animal cells, where the peroxisome instead degrades long chain fatty acids stored in LDs [11]. Further, LDs have been found to interact with lysosomes by way of macroautophagy. Since LDs supply precursors for phospholipid synthesis under nutrient starvation conditions, they initiate the formation of the omegasome precursor of the autophagosome, which then fuses with and is degraded by the lysosome [12].

These interactions and functions described above are applicable to cLDs and not a subset of LDs that are found in the nucleus of certain cells called nLDs. While nLDs share a similar structure to cLDs, there are many relevant differences between them such as their mode of biogenesis, associated proteins, and cellular functions, which I will now outline.

While cLDs are commonly found in all cells, only certain cells form nLDs. They were first described in hepatocytes but have also been found in Caco2 colonic epithelial cells [13-15]. These cells secrete lipoprotein precursors from which nLDs can be generated. This occurs through the accumulation of ApoB-free luminal LDs in the ER that enter the nucleus of cells through type I nuclear membrane invaginations that rupture the inner nuclear membrane [16]. However, nLDs have also been found in U2OS osteosarcoma cell that do not secrete lipoprotein [17]. This indicates more than one mechanism of nLD biogenesis, which will be discussed later. Moving away from mammalian tissues, nLDs have been found in yeast cells as well as in *C. elegans* intestinal and germ cells [18], indicating that nLDs are evolutionarily conserved in many different species. While the exact function of nLDs in the cell is not currently apparent,

they must have an important role given their evolutionary history in two different phylogenetic kingdoms.

1.3 Comprehensive Description of Lipid Droplet Categorization

LD research has identified different categories and subcategories of LD classification (**Figure 1.1**). First the classification of LD is used liberally to refer to any phospholipid monolayer that surrounds a rich TAG core regardless of its location in the cell. There are three further subcategories of LDs which specify location within the cell: cytoplasmic lipid droplets (cLDs), nLDs and nucleoplasmic reticulum-luminal lipid droplets (eLDs). Within the context of nLD research, cLD will be commonly used to distinguish the cytoplasmic and luminal forms when this distinction is important. However, within the context of cLD research, this disambiguation is rarely made as cLDs are referred to as LDs due to being the first established LD.

The classification of nLD can then be understood in terms of location within the nuclear compartment. Type eLDs are contained within the nuclear envelope but bud into the nucleoplasm. Since they are not wholly in the nucleoplasm, they are not nLDs. Type II eLDs are actually cLDs that are outside of the nucleoplasm but occupy space within the nucleus through type II NR invaginations. Lastly there are nLDs which are fully in the nucleoplasm and not associated with the nuclear envelope. The distinction between a type I eLD and an nLD can be made by probing with a marker for the inner nuclear membrane (INM), such as lamin B1 receptor (LBR). If the LD is within a LBR ring, it is a type I eLD whereas LDs outside of them are nLDs. Though, it is possible that a type II eLD may appear to have an LBR ring from the folds of the NR invagination if there is not enough imaging resolution. Probing with LBR is specifically useful, as some nLDs

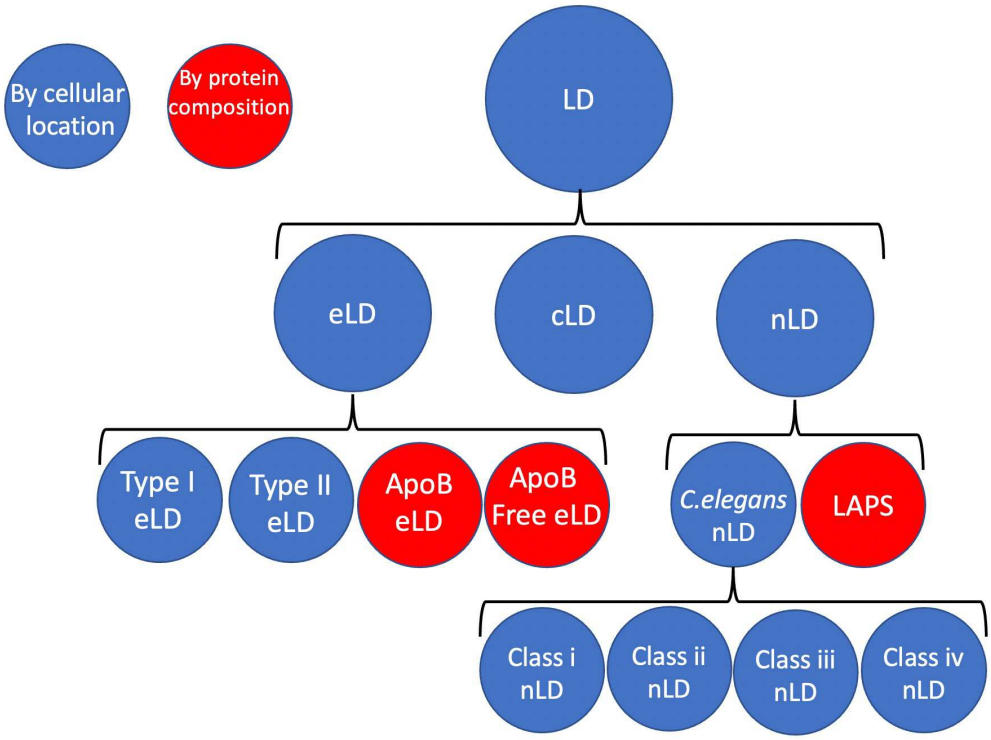

Figure 1.1. Nested Classification Structure of LDs and Subcategories. A Lipid Droplet (LD) is the main term used for either nucleoplasmic reticulum-luminal lipid droplet (eLD), cytoplasmic lipid droplet (cLD), or nuclear lipid droplet (nLD). nLDs have another subcategory called lipid associated PML structures (LAPS). The colour of the circles indicate if their classification is determined by its location within the cell (blue) or by the proteins that associate with it (red).

associate with the nuclear lamina. Since LBR is a transmembrane protein, it should not encompass nLDs when visualized by immunofluorescence (IF).

The contextualization of eLDs can also be further refined. Sołtysik et al. (2019), identified two different pools of eLDs, primordial apolipoprotein B100 (ApoB)-containing particle or ApoB-free LDs. This distinction is important as nLDs are derived from ApoB-free LDs, which are precursors to very low-density lipoprotein (VLDL) [16].

The classification of nLDs can then be understood at the level of unique protein interactors. Two different papers have made subcategories of nLDs**.** The first is lipid associated PML structures (LAPS). This category of nLDs are associated with PML, where they contain more DAG since they are enriched with CTP: phosphocholine cytidyltransferase (CCTα) and phosphatic acid phosphatase (Lipin1; a.k.a. PAP), and are deficient in canonical PML-NB proteins small ubiquitin like modifier (SUMO), death domain-associated protein 6 (DAXX) and SP100 [19].

The other nLD distinction comes from a recent nLD study performed in *C. elegans* from Mosquera et al, (2021). Here the researchers proposed a model of various classes of nLDs based on observations relevant to their research. This proposed class system is not to be confused with the other class system for luminal LDs. Class i nLDs form on the INM and bud fully into the nucleoplasm but split the peripheral heterochromatin from the nuclear lamina. This is in contrast with class ii nLDs (also described as kernel vesicles), which are coated by both the heterochromatin and lamin instead of just the heterochromatin. The simplest is class iii, which does not associate with either heterochromatin or the nuclear lamina as they originate from INM tubules. Lastly type iv nLDs where proposed to originate from the in pocketing of INM tubules.

What differentiates type iv nLDs from type iii is that rupture of the tubule formed around the nLD leaves remnants of the tubules that still associate with the nLD [18]. Though this study was performed in *C. elegans*, the conserved nature of nLDs from yeast to humans indicates that this categorization could also be conserved.

1.4 Lipid Droplet Formation

While the formation of cLDs is well understood, the same cannot be said for nLDs. The synthesis of cLDs involves the accumulation of TAG in the ER by the combined activities of glycerol 3-phosphate acyltransferase (GPAT), 1-acylglycerol 3-phosphate acyltransferases (AGPAT), Lipin1, and diacylglycerol acyltransferase (DGAT) [20]. GPAT and AGPAT sequentially attach long-chain acyl-CoA thioesters to glycerol-3 phosphate and lysophosphatidic acid, respectively, to form phosphatidic acid, which is then dephosphorylated by lipin to form diacyl glycerol (DAG). Another long-chain acyl-CoA thioester is then attached to DAG to create TAG. The formation of DAG and TAG is coordinated by the seipin and lipid droplet assembly factor 1 (LDAF1) in between the two leaflets of the ER [21]. The cytoplasmic facing leaflet begins to form a lens and balloons out into the cytoplasm through the continued funneling of TAG and DAG into the nascent cLD facilitated by seipin. While the cLD is still attached to the ER membrane, proteins from the ER can move to the nascent cLD (termed class I proteins), such as GPAT, AGPAT, and DGAT [22, 23]. The accrued lipid biosynthetic enzymes continue to facilitate TAG synthesis and cLD budding. Once separated from the ER, the cLD can then recruit a second wave of proteins from the cytosol (class II LD proteins) such as perilipins, which associate the surface monolayer of the mature cLD [24].

While nLD biogenesis is different from that of cLD, they share a few similarities (**Figure 1.2**). Namely the proteins GPAT, AGPAT, Lipin and DGAT proteins also coalesce at the inner nuclear membrane and are required for nLD biogenesis [16, 19]. While seipin facilitates the formation and maturation of cLDs, nLDs form in a seipin-independent manner in U2OS cells through the accumulation of TAG and DAG at the INM [16]. This process of lipid droplet lensing and budding into the nucleoplasm is only described for nLD biogenesis in U2OS cells.

This seipin-independent mechanism is not shared across all species, however. In yeast, nLDs form in a seipin-dependant manner that is ostensibly the same mechanism used in the cLD biogenesis [25]. The role of seipin in nLD formation is perhaps indicative of nLD evolutionary history. For example, the amoeba *D. discoideum* expresses a seipin homologue that does not localize to the ER to form cLDs but does not form nLDs [26]. This might indicate that there was a transitionary evolutionary event that first required a seipin-like homologue to from nLDs before being able to transition to seipin-independent mechanisms.

Another mechanism of nLD biogenesis occurs in cells that secrete lipoproteins, such as hepatocytes and intestinal epithelial cells. Under conditions of ER stress, eLDs that are chylomicron precursors that coalesce with apoB-containing dropelts to form mature lipoproteins instead translocate to type-I NR invaginations of the INM [16]. eLDs in the nucleoplasmic reticulum are depleted of lamin A, lamin B receptor and SUN1/2 [16, 17]. The eLD then enters the nucleoplasm proper to become a nLD in a PML-II dependant manner [17]. From here various lipid biosynthetic enzymes are recruited to the

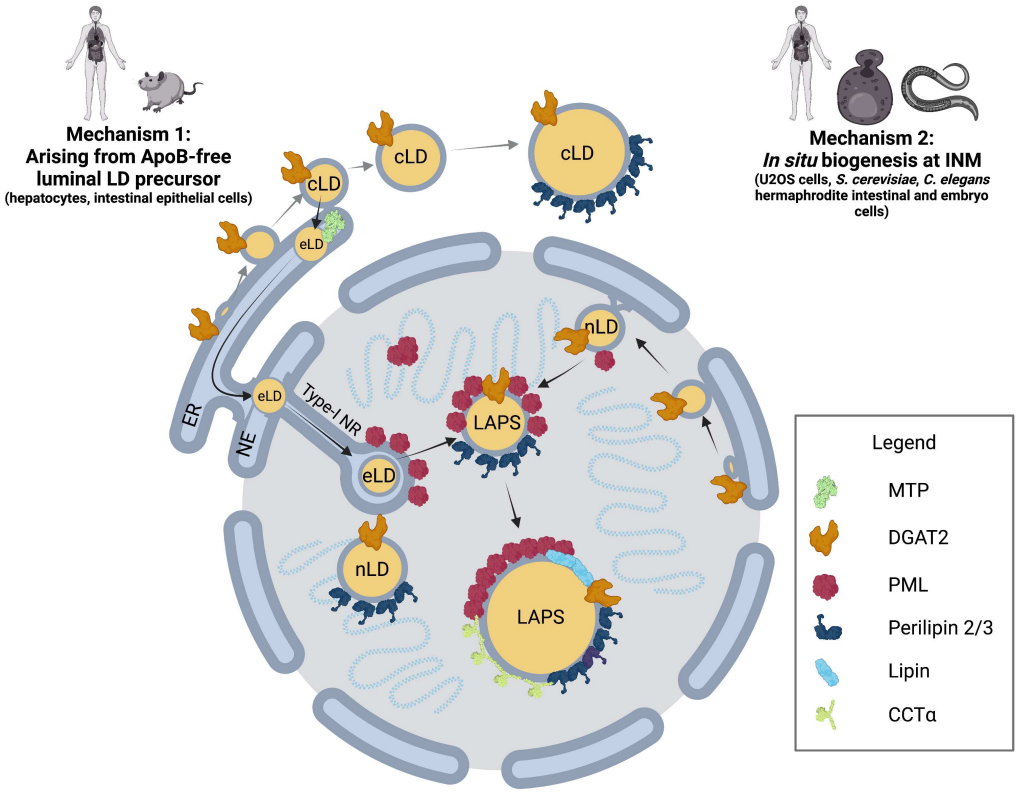

Figure 1.2. Schematic of nLD Biogenesis and LAPS Formation. nLD biogenesis occurs through two mechanisms. Mechanism 1: ApoB-free eLDs form in the ER and migrate to type-I NR invaginations. PML-II localizes to sites of lamin deficiency, aiding the egress of the eLD into the nucleoplasm though ruptures in the membrane. Free of the NR membrane this LD is classified as a nLD. Mechanism 2: TAG synthesis occurring at the INM facilitates the lensing and budding of LD into the nucleoplasm. This process is Seipin dependant in *C. elegans*, and seipin independent in mammals. If PML is associated with nLD, it is denoted as a LAPS.

nLD surface. Both DGAT2 and CCTα are recruited and promote nLD maturation and growth through the production of TAG and phosphatidylcholine (PC) [16, 17].

1.5 Nuclear Lipid Droplet Function

Given that nLDs are physically sequestered from their cytoplasmic counterparts, this provides us insights to the possible functions of nLDs. Firstly, nLDs are unlikely to be energy storage depots since they are sequestered in the nucleus away from mitochondria, and are smaller with less TAG compared to cLDs [13]. This discrepancy in composition and size is indicative of a greater surface-to-volume ratio of nLDs. One possible function of nLDs is to provide ER stress relief during an overload of fatty acids and lipotoxicity by the recruitment of CCTα to nLDs to increase PC synthesis. This allows the cells to 1) increase ER expansion and 2) increase the formation of more phospholipids for incorporation into the monolayer [27]. The recruitment of CCTα to nLDs serves to activate CCTα when it is embedded in nLDs [15]. CCTα is the rate-limiting enzyme in PC synthesis and catalyses the synthesis of CDP-choline from phosphocholine [28]. From there choline/ethanolamine phosphotransferase (CEPT) catalyzes the final reaction to form PC from CDP-choline. The increased PC synthesis relieves ER stress by increasing the volume of the ER to accommodate unfolded proteins caused by ER stress. Another way to mitigate ER stress is the formation of more phospholipid monolayer components of cLDs which would sequester the excess TAG. The newly formed cLDs could then be used by the cell as an energy source.

There is also evidence that nLDs can affect gene expression by two potential mechanisms: 1) regulation of chromatin structure and 2) activation of nuclear

transcription factors [27]. nLDs regulating gene expression through chromatin organization was hypothesized due to the site of nLD formation and their associated proteins. eLDs break through regions of the INM where there has been lamina depletion, which causes changes in histone methylation and, in turn, epigenetic modifications to the chromatin [29, 30]. Further, the PML-NB associated protein DAXX is a H3.3 histone chaperone [19, 31]. The recruitment of H3.3 histone to its chaperones that associate with PML-NBs is DAXX-dependant. When PML associates with nLDs to form LAPS, DAXX was one of the canonical proteins that dissociates. This indicates that nLD formation is potentially involved in the epigenetic gene regulation through differential DAXX-mediated H3.3 histone associations.

Another way nLDs can regulate gene expression is by activation of the nuclear transcription factor co-activator lipin-1, which is recruited to nLDs in U2OS and Huh7 cells. In addition to its phosphatidic acid phosphatase activity, lipin-1 interacts with transcription factors such as peroxisome proliferator-activated receptor α (PPARα) and its coactivator, PPAR gamma coactivator 1 (PGC-1α) [32]. These transcription factors are important in regulating cellular energy metabolism by activating genes involved in gluconeogenesis and fatty acid oxidation [33]. Lipin-1 can also act as a repressor to the master regulator of lipid homeostasis, sterol regulatory element-binding protein (SREPB). When phosphorylated by active mammalian target of rapamycin complex 1 (mTORC1), lipin remains cytosolic and does not inhibit SREBP transcriptional activity [34]. However, dephosphorylated lipin-1 enters the nucleus and causes structural changes resulting in elongated nuclei. This conformational change inhibits SREBP transcriptional

activity, in turn suppressing lipogenesis by the downregulated expression of key fatty acid and cholesterol metabolic genes.

An outstanding question in LD research is the relation of nLD size to its function. As pointed out earlier, the composition of LDs leads to changes in surface area-to-volume ratio. Fewer but larger LDs maximizes volume, whereas many smaller LDs maximizes surface area. This is an important perspective to understand as it will outline the model that size defines the function for LDs.

A recent LD paper by Bosch et al. (2020) demonstrated that in response to bacterial infection or lipid polysaccharide treatment, mouse hepatocytes had more, smaller cLDs than untreated/uninfected cells. This indicates that maximizing surface area of LDs is being favoured by the cell by way of a metabolic shift in surplus LD surface phospholipids. When accompanied by the data that antiparasitic, antiviral and GTPases associate with LDs, this indicates that LD size is being regulated to modulate LD size in order to serve a cellular function, in this case protein recruitment to the LD surface [35].

Putting this into the perspective for nLDs, two different metabolic enzymes associate with the droplets: CCTα and lipin-1 [19]. What is interesting about these two enzymes is they both catalyze the formation of opposing components used for the formation of LDs. CCTα is the rate limiting enzyme for PC synthesis, which would be incorporated into the phospholipid monolayer [36]. Lipin-1 catalyzes the formation of DAG, which forms TAG that is incorporated into the LD core [37]. With the former understanding that regulating LD size is important for the function of the LD itself, we

can then apply this framework to see how these two enzymes are interacting to regulate nLD size.

In the case of CCTα, the synthesis of PC favors the maximization of surface area. This would mean a function of CCTα is to generate more smaller nLDs. This is supported by results from CCT KO cells which have both fewer and larger nLDs. Comparing this with the lipin-1 analysis from the same paper, there were fewer lipin positive nLDs but they were also statistically larger [19]. These data show that nLD size can be regulated through the biosynthetic enzymes on their surface. Lipin-1 and CCT would then regulate the ability of other proteins to associate nLDs by changing their size.

Extrapolating from cLD studies that demonstrated ATGL is an important regulator of LD size by a COP coatomer-dependant mechanism [38], it seems this same mechanism could be used in nLDs. Based on the recent study using *C. elegans* that showed COP-I coatomers interacting with nLDs [18], it is plausible the same mechanism is at work in nLDs. Further validation of the COPI/ COPII coat proteins as well as ATGL interaction with nLDs would not only identify new proteins to the nLD proteome, but also validate this model.

1.6 nLDs vs cLDs – Structure, Location, and Composition Comparisons

Nuclear lipid droplets (nLDs) are a unique nuclear domain since they have a protein and lipid composition that is distinct from both the nuclear environment as well as their cytoplasmic lipid droplet (cLD) counterparts. While it is obvious that an organelle composed of phospholipids, TAG and CE would have a greater lipid-to-protein ratio than

the nucleus as a whole, the types of lipids are different. While the nucleus is mostly composed of polar lipids (glycerophospholipids and sphingolipids), with traces of TAG, CE, and cholesterol, nLDs are enriched in these hydrophobic lipids with less polar lipids [13].

Further the structure nLDs is different from the cLDs. Comparatively, cLDs contain far more lipids while having less protein than nLDs. This is most likely a function of cLDs being larger, which would increase the volume to surface area ratio [13]. This in turn skews the lipid composition percentage of cLDs which are mostly composed of TAG, with very little cholesterol esters, cholesterol, and polar lipids while nLDs have a more equal proportion of each. Only in part could this difference in composition be explained by variation in sizes between nLDs and cLDs.

The spatial difference between cLDs and nLDs is also important for understanding why nLDs are unique. Since cLDs are formed on the ER, which is continuous with the nuclear envelope, it was proposed that nLDs could just be cytoplasmic LDs trapped in an invagination of the nuclear envelope [13, 14]. For nLDs to be a distinct nuclear subdomain, there needed to be evidence of LDs in the nucleus and not connected to the nuclear envelope. From serial sections of human liver tissue, it was shown that a small fraction of LDs in the nucleus were not connected to the nuclear envelope, with varying amounts of heterochromatin association [14]. However, some cLDs associate with the nucleus and are enveloped in an invagination of the ER [14].

Another protein involved in lipid regulation found exclusively on nLDs is perilipin-3 [18,19]. What is important about this protein is that another member of the

family, perilipin-2, is constitutively found on cLDs, but absent from nLDs [17]. For cLDs, the function of perilipin-2 is to coat the surface of the LDs and protect it from hydrolysis, thus altering lipid metabolism through preserving the lipid stores [39]. However, when perilipin-3 coats the surface of nLDs, it competes with CCTα for nLD surface binding. Since CCTα regulates PC synthesis through its activation by membrane binding, perilipin-3 acts to reduce the number of nLDs [16]. These two mechanisms serve to further differentiate the proteomes of cLDs and nLDs, but also the different roles of perilipins for preserving cLDs by reducing lipolysis and reducing nLD formation by blocking PC synthesis.

The regulation of nLD lipid synthesis is not just tailored towards phospholipid synthesis, but also involves other glycerolipids. Lipin-1 catalyzes the cleavage of phosphatidic acid to form diacylglycerol and is found on nLDs [19]. The formation of DAG is important as it acts as a substrate to DGAT to form TAG [37] and CEPT to form PC through the Kennedy pathway [40]. Further, DAG activates CCTα in a feed forward mechanism to enhance PC synthesis [41].

Continuing the theme of nuclear lipid synthesis, DGAT2 is also present on nLDs [17]. This is important as both possible fates for DAG occur on nLDs; DAG made from lipin-1 can be turned into TAG by DGAT2 or the DAG can enter the Kennedy pathway to become PC in the ER (**Figure 1.3**). Both these possible outcomes for DAG are important as this means the machinery required to make the structural components for LDs — the outer phospholipid monolayer or the inner neutral lipid core — are present on nLDs.

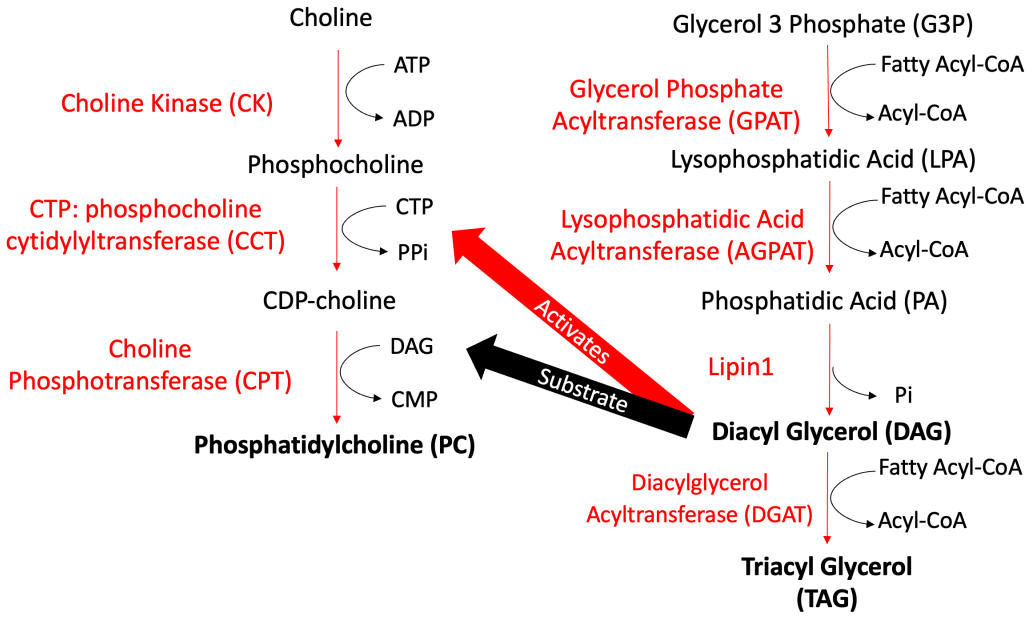

Figure 1.3. Biosynthetic Pathway of PC and TAG Pathways and their Interconnections. When DAG is produced by Lipin1, the pathway bifurcates. Either the DAG can enter the Kennedy pathway and become PC or continue to become TAG.

While the previous information comes from mammalian cell models, a recent study identified nLDs in *C. elegans*, which are more closely related to mammals than yeast. Firstly, Mosquera et al. (2021) found that the nLDs in the intestinal nuclei were associated with bundles of microfilaments (nuclear actin) and membrane tubules. These microtubules that associates with the nLDs seemed to originate from either the inner nuclear membrane or from extensions of membrane vesicles. Further, it was shown that some nLDs were contained in sacs of either lamina, heterochromatin, or both. These sacs when degraded caused damage to the intestinal nuclei, which the cell would then repair. Where the largest fat deposits were correlated with nLDs and the most cellular damage. Further the authors showed that mutations in the genes SEIP-1, NEMP-1, COPA-1, and COPB-2 effected the prevalence of nLDs in germ cells. Additionally, worms with NEMP-1 and SEIP-1 mutations had increased nLD diameter [18]. SEIP-1, which encodes for the protein seipin, therefore has a role in nLD formation in worms. The role of the protein NEMP-1 (aka TMEM194a) is a bit more cryptic. This protein is without a clear function but does localize to the nuclear lamina, which is relevant given the finding that showed a subgroup of nLDs being contained within sacs of the nuclear lamina [18]. Lastly, COPA-1, and COPB-2 code for the COP coat proteins in vesicular transportation [42]. Both COP-I and COP-II mediate the delivery of adipose triglyceride lipase (ATGL) and perilipin-2 to cLDs [38]. This is important as the recruitment of ATGL to nLDs might mean that this enzyme hydrolyzes TAG on nLDs and could be coordinated with TAG synthesis. Though perlipin-2 has been shown not to associate with nLDs, it would be interesting to see perilipin-3 recruitment to nLDs is COP-I and COP-II dependant.

1.7 PML Structure and Relationship to nLDs

nLDs were first identified to associate with the protein PML. To better understand this subset of nLDs that associate with PML, a review of PML is required. PML belongs to the family of tripartite motif (TRIM) proteins that contain a conserved RING finger/ B box/ coiled coil (RBCC) domain [43]. The PML gene contains 9 exons that can be spliced into 7 different isoforms. Six of these isoforms are nuclear and can form self-associating structures call PML-nuclear bodies (PML-NBs) [44]. PML-NBs are scaffolds that recruit a smorgasbord of over 100 different proteins [45]. Due to the collection of associated proteins, PML-NBs have roles in many different cellular pathways such as DNA damage recognition, DNA damage repair, apoptosis, gene expression, immune responses, and post-translational modification [46].

The recruitment of client proteins can occur either through interactions with the RING finger domain or with the many SUMO-interacting motif (SIM) of PML. Initially SUMO machinery interacts with the RING finger domain, such as the universal E2 SUMO-conjugating enzyme UBC9 [47]. These SUMO ligase proteins can then create the second layer of scaffolding to the PML-NBs after proteins have been recruited to the RING domain. By the subsequent SUMOylations that occur on the PML-NBs, the C-terminal SIM can bind the SUMO residues and can then homo multimerize (**Figure 1.4**) [48]. Other proteins with SIM domains or that are SUMOylated are then able to bind to PML-NBs. These interactions between SUMO and SIM occurs though noncovalent interaction that is dependent on the kinase CK2 phosphorylating serine residues adjacent to the hydrophobic core of the SIM motif [49, 50]. This is how PML canonical proteins DAXX and SP100 interact with PML, but also SUMO proteases such as SENPs [51]. The

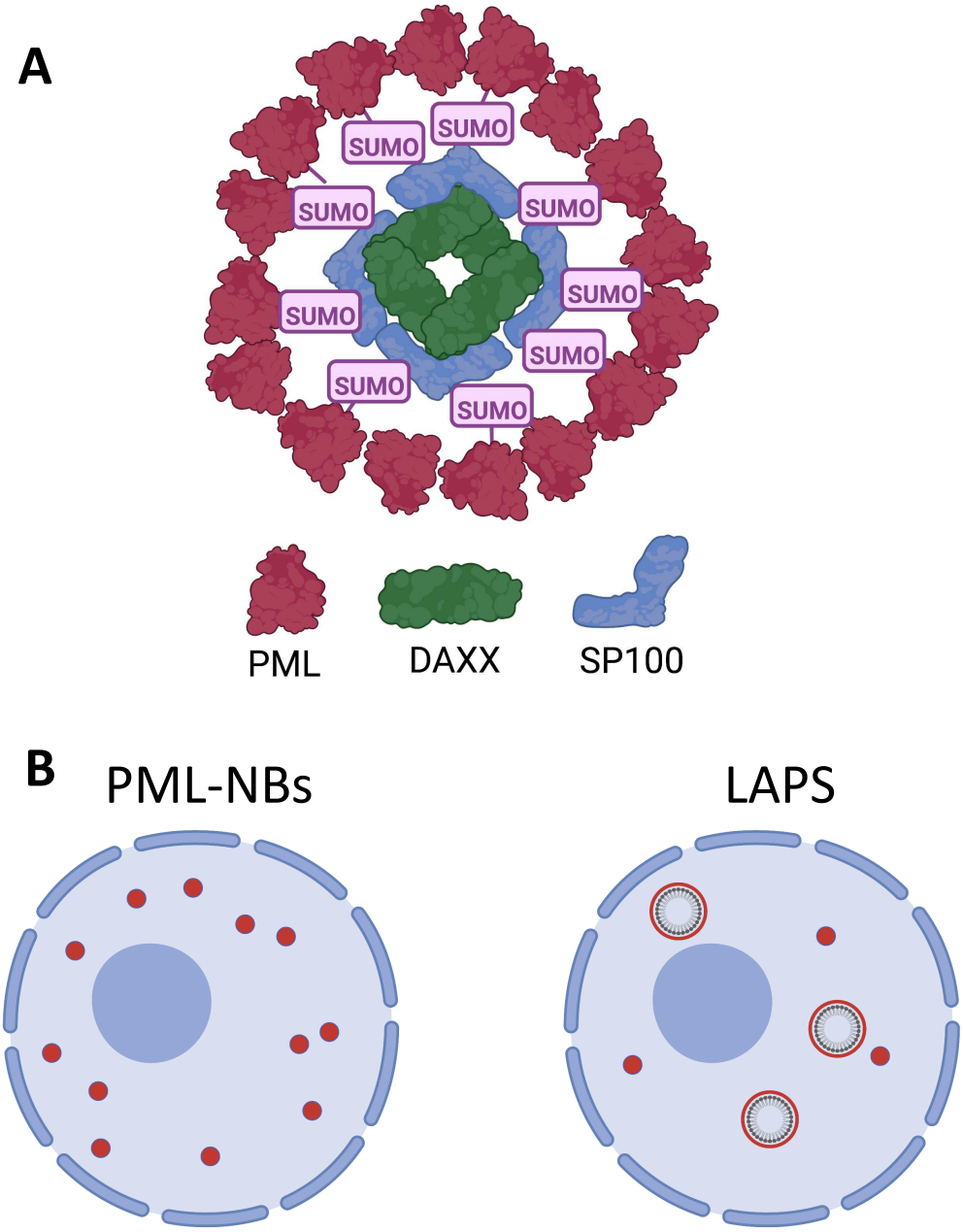

Figure 1.4. Illustration of PML-NB Formation. (A) When SUMOylated, the C-terminal of PML SUMO-interacting motif (SIM) can bind other SUMO residues and homo multimerize forming spherical structures. Other interacting proteins of PML-NBs interact at the center of the nuclear body. **(B)** Under basal conditions, PML forms nuclear bodies throughout the nucleus, which appear as puncta when observed by IF. When under lipid overload, PML will associate with the nLDs to form LAPS. These appear as ring structures when observed by IF.

accumulation of different proteins involved in SUMOylation allow for these PML-NBs to be effective centers for post-translational modification, but also highlight how PML is able to act as a scaffold protein and interact with many different proteins.

What makes LAPS interesting with respect to PML is that they lack three proteins that are well established interactors of PML-NBs, SUMO, DAXX and SP100. Since LAPS are poorly SUMOylated, the absence of these proteins is explained through their SUMO dependant interactions with PML-NBs [19]. In hepatic Huh7 cells, it was determined by siRNA knock down that PML-II was required for nLD formation [17]. This complements the data that showed that the PML-II isoform was associating with the INM at points of lamina depletion and nLD biogenesis. The same study also identified that nLDs increased with the siRNA knock down of the proteins SUN1, a component of the LINC complex that connects the interior of the nuclear envelope to the cytoskeleton, and REEP3/4, which facilitates the separation of nuclear envelope components away from chromatin during mitosis [17, 52, 53]. The authors suggested that PML-II was tethering nLDs to the INM and that SUN1 and REEP3/4 were serving to clear the nucleoplasm of nLDs during mitosis, an interaction that occurs downstream of PML-II inducing nLD formation. In U2OS cells, siRNA knock down of PML-II did not affect nLD number or size, but CRISPR/Cas9 mediated knock out caused a 50% reduction in nLDs [19]. This indicates that partial depletion of PML-II is insufficient to stop nLD formation.

Based on 3D surface reconstruction of LAPS in U2OS cells, it was observed that PML and CCTα associate at different locations on LAPS [19]. While there is no evidence of PML and CCTα directly interacting with each other, they both do associate with

nuclear lamina threads. The accumulation of farnesylated prelamin A causes massive conformational changes to the nucleus resulting in multiple nuclear invaginations that form these thread-like structures. This occurs commonly in Hutchinson–Gilford progeria syndrome (HGPS), and results in lipodystrophy and early aging. In HGPS cells, the accumulation of prelamin-A changes the location of PML and CCTα to the type-1 NR [54, 55]. These sites could then serve for nLD biogenesis allowing for both PML and CCTα to accumulate on the nascent nLD.

PML is also integrated with lipid metabolism and homeostasis through its interaction with SREBP, a master transcriptional regulator of sterol and fatty acid synthesis. A study demonstrated that in metastatic human prostate cancers, *PML* was often co-deleted with the tumour supressing gene *PTEN* [56]. In mouse models that were *Pten*-null and had PML deleted to form the double-null phenotype, SREBP was hyperactivated leading to the formation of a lethal metastatic tumour [57]. A dissimilar result happened in triple negative breast cancer cells, where PML was demonstrated to have an oncogenic effect by promoting fatty acid oxidation [58]. PML reduced PGC1A acetylation, activating the enzyme resulting in PPAR dependant fatty acid oxidation. Though PML has two different effects on tumour suppression, it does so by altering lipid metabolism and homeostasis.

1.8 Lipid Droplet Related Diseases

Given that nLDs form during fatty acid overload (i.e., oleate treatment), it is not surprising that there are pathological connections. While there is limited evidence that

nLDs are directly involved in a disease pathology, we can take inference from research performed on cLDs. The main sources of LD pathologies stem from lipid overload, namely hepatitis C virus (HCV), non-alcoholic fatty liver disease (NAFLD), and the connections between obesity and diabetes with NAFLD. In the following section I will outline these connections between these pathologies and LDs.

The first connection for nLDs to disease came from an electron microscopy (EM) study of serial sections of liver taken from a patient with a chronic HCV infection showing nLD formation [14]. HCV remodels host cells lipid metabolism to favour increased lipogenesis and reduced lipid secretion and β-oxidation, a metabolic state that would favour nLD formation through the accumulation of lipids [59, 60]. Further, VLDL is required for HCV infection, which might be indicative of the biogenesis of the nLDs in the patient's liver occurring through the VLDL precursors egressing through the type-I NR invaginations of the INM.

The disease most correlated to cLDs is NAFLD, a disease characterized by the presence of LDs in hepatocytes [61]. The first stage of the disease is steatosis but can progress to non-alcoholic steatohepatitis (NASH) resulting in inflammation and hepatocellular ballooning and irreversible hepatic injury [62]. The progression of NAFLD occurs by a feed forward mechanism. The excess LDs that form beget more LDs, in turn increasing the total number of LDs. If there is a high percentage of intracellular lipids that cause negative membrane curvature, it leads to the embedding of the cLD into the ER [63]. This prevents access of surface proteins to access the lipid core and prevents regulation of the LD protein composition resulting in ER-stress and inflammation. Further BasuRay et al. (2019) describe that mutations to the protein

patatin-like phospholipase domain-containing protein 3 (PNPLA3) have been found to result in NAFLD. Wild type PNPLA3 acts as a TAG hydrolase and is normally degraded by ubiquitination. However, if the isoleucine is mutated at the 148 site to a methionine, the protein has reduce enzymatic activity and is not degraded. This results in the accumulation of the dysfunctional protein onto the surface of LDs, resulting in larger and more LDs. This specific mutation is associated with NAFLD and higher risks of the patient developing hepatic fibrosis [64]. Lastly, perilipin 2 (PLIN2) is a protein that promotes lipid storage and is upregulated in patients with NAFLD [65, 66]. Given this continued upregulation from the NAFLD, PLIN2 coats the outsides of the LD monolayer and prevents lipolysis by preventing access of adipose triglyceride lipase (ATGL) to the hydrophobic core. This creates a feedback mechanism resulting in the proliferation of more LDs [67]. Mutation at the 251 serine when mutated to proline in humans was found to have increased build-up of smaller LDs that were associated with NASH [68]. These symptoms were also associated with symptoms of dysfunctional insulin signalling [69].

What is particularly interesting about NAFLD is that both obesity and diabetes are all comorbidities of one another. Through the lens of obesity, calorie surplus resulting in excess storage of energy as TAG leads to the accumulation of hepatic LD formation characteristic of NAFLD. The increased lipid storage also increases the burden of insulin signalling, which would lead to type -II diabetes [70]. Likewise, obesity has been shown to progress HCV with weight loss causing a reduction in steatosis [71]. This shows the importance of LDs and their connections to diseases. Improper lipid storage from either obesity, diabetes or NAFLD, all have associated insulin resistance stemming from disruption of lipid homeostasis [72-74] . However, it is not clear if nLDs are directly

involved with obesity, diabetes, or NAFLD. If nLDs are sites of lipid metabolism regulation, then they would be potential targets for therapy development.

1.9 Proximity Labelling

In order to study how proteins interact with one another spatially and temporally, proximity labelling can be used. The premise is that conjugating a proximity labelling protein to your protein of interest (i.e., the bait) will identify adjacent proteins (i.e., the prey) that interact in the context of an intact cell. Using various microscopy or mass spectrometry-based methods, one can then identify prey proteins that interact with the bait. The approach invovles two different methodologies, peroxidase-based or biotin ligase-based proximity labelling. While there are multiple proteins in each category, I will be focusing on the advantages and disadvantages of using the proteins APEX2 and BirA for each category respectively.

APEX2 is an engineered 28 kDa ascorbate peroxidase derived from soybean designed by Lam et al. (2015). Using directed evolution on the first-generation APEX protein, they selected for mutations that were most effective at biotinylating surface membrane protein in yeast models. This resulted in a more active and sensitive enzyme, which was a limitation of the first-generation APEX. There were also improvements in the enzyme kinetics, thermal stability, and resistance to high H_2O_2 concentrations. The last improvement is important due to the use of H_2O_2 in the biotinylation reaction (**Figure 1.5**). The reaction itself involves pre-treating cells with biotin-phenol and brief exposure to H_2O_2. APEX2 enzyme uses H_2O_2 to oxidize the biotin-phenol into a phenoxyl radical,

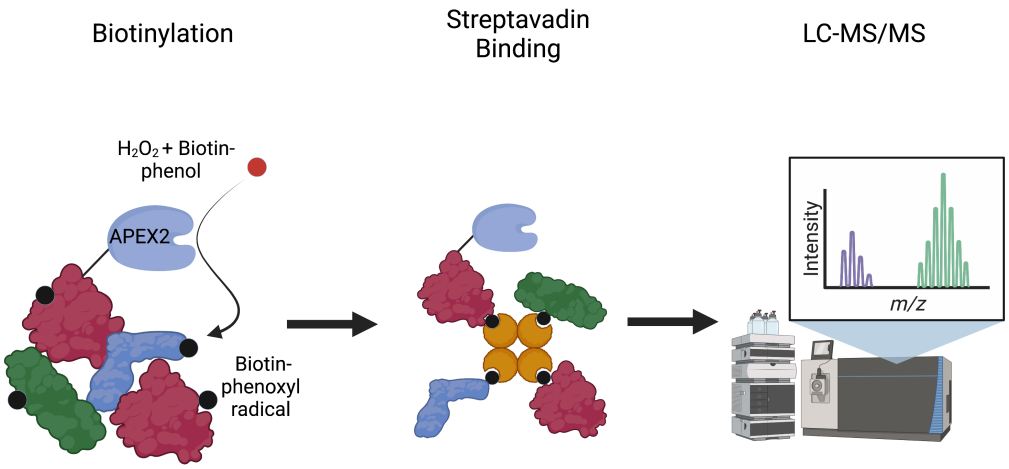

Figure 1.5. Schematic Proximity Labelling Experiment. A fusion protein consisting of the protein of interest (bait protein) is conjugated to APEX2. When in the presence of exogenous H_2O_2 and biotin-phenol, APEX2 oxidize the biotin-phenol into a phenoxyl radical which reacts with nearby adjacent proteins (prey protein) labelling them. The prey proteins that have been labeled can then be enriched by using streptavidin which binds to the biotin molecules now attached to the prey proteins. The enriched sample can then be sent for LC-MS/MS analysis to determine their identities.

which conjugates with tyrosine, tryptophan, cysteine, and histidine residues in closely associated proteins [75]. What is unique about this reaction is its relatively short incubation time (1 minute) and small labelling radius (20 nm) [76].

BirA is a 35 kDa engineered biotin ligase derived from *E. coli* designed by Roux et al. (2012). This protein has a single site mutation that allows better exchange of the activated biotin with the enzyme's active site and promotes interaction with amines on nearby exposed lysine residues. BirA catalyses the formation of biotinoyl-5′-AMP using endogenous ATP and exogenous biotin [77]. The major difference is the reaction time of the enzymes, which is up to 24 h for BirA and minutes for APEX2. Further, there is a reduced number of amino acids that can be labelled by BirA and it is larger protein, which can interfere with protein-protein interactions. BirA also has a smaller labelling radius of 10 nm [78]. Nevertheless, the same methods of prey detection and identification are used for both.

A recent paper by Barroso-Gomila et al. (2021) investigated interactors of PML-NBs with proximity labelling using a modified BirA enzyme called TurboID. This enzyme is the same size as BirA but has an additional 14 mutations that contribute to a reduce reaction time (2 hours). The researchers used a split Turbo-ID method that has the C-terminus of TurboID attached to SUMO and the N-terminus attached to PML. This results in activation of TurboID only when the two halves were in close proximity of each other on PML-NBs. It should be noted, however, that some residual biotinylation activity remains in the N-terminal half. This proximity labelling strategy was dubbed SUMO-ID. The researchers identified multiple proteins that interact with PML involved in SUMOylation, transcriptional regulation, DNA repair and stress response, all of which

are characterized roles of PML. The pool of proteins was also enriched in SIMs and were substrates of SUMO [79].

While this paper identified novel PML-NB interactors, there are a few pitfalls. Firstly, TurboID has issues with protein instability and constant biotinylation without the addition of exogenous biotin even with the split TurboID system [80]. There are also issues with the temporal resolution, which is shorter with APEX2. However, a larger issue is that the experiments only targeted SUMO-dependant PML interactions and not the general PML-NB proteome.

My objective was to expand the PML and LAPS interactome by utilizing the proximity labelling with expression vectors of APEX2 fused with PML isoforms I and II (**Figure 1.6**). This will allow detection of isoform specific interactions with PML, allow for better temporal resolution of proteins that are associated with PML, and potentially reduce background biotinylation in control samples. Further, I performed proximity labelling in cells that have oleate-induced nLD formation, which will give information on this novel lipid domain. Expanding the unique protein composition of LAPS from other PML nuclear bodies will further elucidate what the purpose of nLDs are but also differentiate how nLDs are different from cLDs. The high confidence interactors generated form my proximity labelling experiments will inform the avenues of research linking PML and lipid metabolism. Given the involvement of LDs with many prevalent diseases, such as obesity, diabetes, and NAFLD, understanding the cellular processes that occur when PML is associated with nLDs through protein-protein interactions would give potential insight to research in these fields as well.

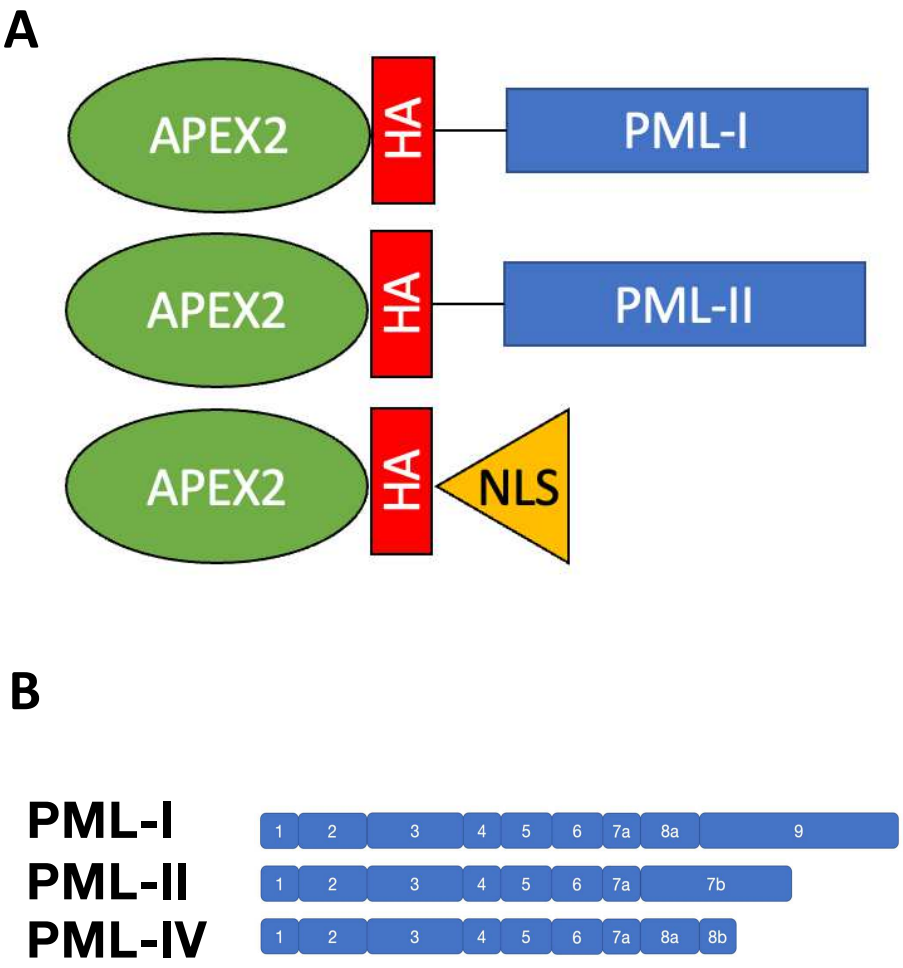

Figure 1.6. Schematic Structure of APEX2-HA-PML Constructs (A) APEX2 was cloned N-terminal of PML or a NLS signal. The C-terminal of APEX2 had a engineered HA tag **(B)** The isoform structure of the PML isoforms I,II, and IV with their respective exons.

Chapter 2: Materials and Methods

2.1 Cell Culture

U2OS, U2OS-PML clover, and U2OS-PML KO cells were cultured in DMEM containing 10% FBS. Huh7 cells were cultured in low glucose DMEM (1 g/L) supplemented with 10% FBS. All cells were cultured at 37°C at 5% CO_2. U2OS-PML clover [81] and U2OS-PML-KO [82] cells were provided by Dr. Graham Dellaire.

2.2 Transfection of Cells

One hundred fifty thousand cells were seeded on 35 mm dishes and allowed to reach 65% confluency. The transfection mixture consisted of 1 μg of purified plasmid and 3 μl of Lipofectamine-2000 in 400 μl DMEM. The mixture was incubated for 30 minutes at room temperature, applied to a dish of cells in 1.5 ml of fresh cell culture media and incubated overnight. Fresh media was replaced the following day with any treatments, such as oleate addition, and cells were harvested 24 h later.

2.3 SDS-PAGE and Western Blotting

Media was aspirated from cells, and they were washed once with 1 ml of ice-cold PBS. Cells were then scraped in cold PBS and collected by centrifugation at 13,000 rpm for 10 mins at 4°C, and the cell pellet lysed with SDS reducing buffer (62.5 mM Tris-HCl pH 6.8, 10% glycerol, 2% SDS, 0.05% bromophenol blue, and 5% β-

mercaptoethanol) on ice for 10 min. Cell lysates were sonicated for 10 sec at 60 kHz before being heated to 90 °C for 3 mins.

Cell lysates were separated in SDS-polyacrylamide gels (8% or 12 %) at 100 V in SDS running buffer (3mM SDS, 200 mM glycine, 25 mM Tris-base, 192 mM glycine, 20% (v/v) methanol). Proteins were transferred to a nitrocellulose membrane in transfer buffer (25 mM Tris-base, 192 mM glycine, 20% (v/v) methanol) at 100 V for 1 h.

Nitrocellulose membranes were incubated in blocking buffer (1:4 dilution of Licor Odyssey TBS blocking buffer in TBS (20 mM Tris-base, pH 7.4, 500 mM NaCl)) for 1 h at room temperature. The conditions for primary antibody incubations are indicated in figure legends. Secondary goat anti-mouse (1:20000) and goat anti-rabbit (1:15000) antibodies conjugated to Licor680 or Licor800 IR dye or streptavidin conjugated Licor800 IR dye (1:1000) were incubated with nitrocellulose membranes for 1 h at room temperature. Nitrocellulose membranes were imaged using a LI-COR Odyssey scanner and the fluorescence quantified using the LI-COR Odyssey software V3.0.

2.4 Immunofluorescence

Cells were seeded on 1-mm thick glass coverslips and fixed with 4% (w/v) paraformaldehyde in PBS for 15 min with gentle shaking at room temperature. The cells were then permeabilized using 0.1% Triton X-100 in PBS for 10 min with gentle shaking at 4 °C and then blocked with 1% bovine serum albumin (BSA) in PBS (PBS/BSA) for 1 h at room temperature. Cover slips were incubated with primary antibodies, anti-HA

mouse antibody (Mab) (1:1000), anti-PML Mab (1:200), anti-PML rabbit antibody (Rab) (1:2000), anti-Flag Mab (1:1000) or anti-MK2 Rab (1:200), BSA/PBS (1 ml per well in 6-well dishes) overnight at 4°C. After removal of the primary antibody and washing in PBS/BSA, secondary goat anti-rabbit and goat anti-mouse conjugated to AlexaFluor488 (1:4000), AlexaFluor594 (1:4000), AlexaFluor647 (1:4000) or Streptavidin conjugated AlexaFluor488 (1:1000) in BSA/PBS were incubated with coverslips at 1 h at room temperature. For lipid staining, BODIPY 493/503 fluorophore (1:1000), LipidTOX neutral red (1:1000), and LipidTOX deep red (1:1000), were diluted in PBS and 1 ml added per well to 6-well dishes for 1 h at room temperature. For nuclear staining, Hoechst (1:1000) was prepared in PBS and 1 ml was added per well to 6-well dishes for 5 min at room temperature. Coverslips were mounted on glass slides using Mowiol and subsequently imaged using a Leica SP8 confocal microscope with a 63x oil immersion HC Plan APOCHROMAT objective, 405 nm, 488 nm, 552 nm, and 638 nm lasers, and Lecia LAS X software.

2.5 Preparation of Oleate/BSA Complex and Treatment of Cultured Cells

Oleate BSA (6.6/1) complexes were prepared by dissolving 45 mg of oleic acid into 1 ml of ethanol. Fifty μl of 5 M NaOH was added to the mixture, whereafter the ethanol was evaporated under nitrogen. The oleate was then dissolved in 5 ml of 150 mM NaCl and heated for 4 min at 60°C prior to adding 6.25 mL of cold 24% (w/v) fatty acid free BSA dissolved in 150 mM NaCl. The final volume of the mixture was adjusted to 12.5 mL with 150 mM NaCl to produce a final oleate concentration of 12.7 mM oleate.

After cells have been transfected for 24 h or the day before the cells are to be harvested, the media was replaced and then supplemented with 500 μM oleate/BSA for 24 h and incubated at 37 °C at 5% CO_2.

2.6 Construction of APEX2 Plasmids

To create the APEX2-PML plasmids, APEX2 was amplified from pUC57-APEX2-HA with primers encoding 5' Nhe1 and 3' Bsrg1 restriction sites (See section 2.14). The APEX2-HA plasmid was provided by Dr. Van der Spoel [83]. The amplified DNA was then cloned into pCR Blunt II-TOPO (Invitrogen). The APEX2-HA cassette was released from the plasmid by digestion with Nhe1 and Bsrg1 and the fragment was cloned in frame to pEGFP-C1-PML I and II plasmids that had the GFP cassette released using the same restriction enzymes. These PML plasmids were provided by Dr. Graham Dellaire [81].

To create the APEX2-NLS construct, APEX2 was amplified from puc57-APEX2-HA with a 5' Kpn1 and 3' Bsrg1 restriction sites (See section 2.14). The amplified DNA was then cloned into PCR Blunt II topo (Invitrogen). A clone that was formed in the reverse direction was cut with Xho1 and Bsrg1 and cloned into pEGFP-N1 that had the GFP cassette released using the same restriction enzymes. This plasmid had an NLS previously added using the restriction sites Bsrg1 and Xba1.

2.7 APEX2 Proximity Labelling

Cells were transiently transfected with pAPEX2-HA-PML-I, pAPEX2-HA-PML-II, or pAPEX2-HA-NLS for 48 h. Media containing either 500 µl of oleate or no addition was added to cells 24 h before start of proximity labelling experiments. To commence the biotinylation experiment, 500 mM biotin phenol dissolved in DMSO was added to a final concentration of 0.5 mM in 2 ml of media on 35 mm dishes for 30 min at 37 °C at 5% CO_2. Hydrogen peroxide (30%) was then added to a final concentration of 1 mM for 1 minute at room temperature with gentle shaking. The biotinylation reaction was stopped by the addition of 0.5 ml of quench solution (10 mM Trolox, 20 mM ascorbate in PBS, pH 7). Cells were rinsed an additional two times with 0.5 ml of quench solution. Cells were then lysed according to the methods outlined in 2.3 or prepared for IF according to 2.4.

2.8 LC-MS/MS

The experiments in this section were performed by our collaborator Dr. Francois-Michel Boisvert (Université de Sherbrooke) as in Del Olmo et al. (2019) [84].

2.8.1 Cell preparation

The cell pellet was dissolved in 10 mM HEPES-KOH pH 7.5 and 8 M urea and sonic for 30 seconds (pulse on: 10 seconds, pulse off: 5 seconds) with an amplitude of 25%. The samples were centrifuged at 21,100 x g for 10 minutes at 4°C to remove insoluble debris and the protein concentration was determined by BC Assay.

2.8.2 Reduction, Alkylation and Digestion of proteins

Fifty ug of protein (50 µl in10 mM HEPES-KOH pH 7.5, and 8 M urea) was reduced with 5 mM dithiothreitol (DTT) by heating at 95°C for 2 minutes followed by a 30-minute incubation at room temperature. Proteins were alkylated by adding chloroacetamide (CLAA) (Sigma-Aldrich, Saint-Louis) to a final concentration of 7.5 mM followed by a 20-minute incubation at room temperature in the dark. Urea was diluted to a final concentration of 2 M by adding 50 mM ammonium bicarbonate (NH_4HCO_3). The proteins were digested by adding 1 µg of Pierce MS-grade trypsin and incubated overnight at 30 °C with shaking.

2.8.3 Purification and Desalting of the Peptides on C18 Columns

The trypsin digestion was stopped by adding trifluoroacetic acid (TFA) to a final concentration of 0.2%. The peptides were purified with ZipTip 100 µl micropipette tips containing a C18 column high performance liquid chromatography media (EMD Millipore). The ZipTip was first moistened by suctioning 100 µl of 100% acetonitrile solution three times, then equilibrated by suctioning 100 µl of 0.1% TFA buffer three times. Each peptide sample (200 µl) was passed over the equilibrated ZipTip by suctioning up-and -down 10 times. This step was performed in two steps to pass the entire sample through the column. The ZipTip was then washed with 100 µl of 0.1% TFA buffer six times. Peptides were eluted from the tip into a low protein binding microtube by passing a volume of 100 µl of 50% ACN and 0.1% TFA buffer through the tip 10 times. This step was performed in two batches to obtain a final volume of 200 µl. The peptides were then concentrated in a centrifugal evaporator at 60 °C until completely dry

(~3 h) and then resuspended in 50 µl of 1% TFA buffer. Peptides concentrations were assayed using a NanoDrop spectrophotometer (Thermo Fisher Scientific) and read at an absorbance of 205 nm. The peptides were then transferred to a glass vial and stored at −20 °C until analysis by mass spectrometry.

2.8.4 LC-MS/MS Analysis

For LC-MS/MS, 250 ng of each sample was injected into an HPLC (nanoElute, Bruker Daltonics) and loaded onto a trap column with a constant flow of 4 µl/min (Acclaim PepMap100 C18 column, 0.3 mm id x 5 mm Dionex Corporation). The sample was then eluted onto an analytical C18 column (1.9 µm beads size, 75 µm x 25 cm, PepSep). Peptides were eluted over 2-hour using a gradient of acetonitrile (5-37%) in 0.1% TFA at a flow rate of 500 nL/min while being injected into a TimsTOF Pro ion mobility mass spectrometer equipped with a Captive Spray nano electrospray source (Bruker Daltonics). Data was acquired using data-dependent auto-MS/MS with a 100-1700 m/z mass range, with parallel accumulation-serial fragmentation (PASEF) enabled with a number of PASEF scans set at 10 (1.27 seconds duty cycle) and a dynamic exclusion of 0.4-minute, m/z dependent isolation window and collision energy of 42.0 eV. The target intensity was set to 20,000, with an intensity threshold of 2,500.

2.8.5 Protein Identification by MaxQuant Analysis

The raw files were analyzed using MaxQuant version 1.6.17.0 software [85] and the Uniprot human proteome database (21/03/2020, 75,776 entries). The settings used for the MaxQuant analysis (with TIMS-DDA type in group-specific parameters) were: 2 miscleavages were allowed; fixed modification was carbamidomethylation on cysteine;

enzymes were trypsin (K/R not before P); variable modifications included in the analysis were methionine oxidation, protein N-terminal acetylation and protein carbamylation (K, N-terminal). A mass tolerance of 10 ppm was used for precursor ions and a tolerance of 20 ppm was used for fragment ions. Identification values "PSM FDR", "Protein FDR" and "Site decoy fraction" were set to 0.05. Minimum peptide count was set to 1. Label-Free-Quantification (LFQ) was also selected with a LFQ minimal ratio count of 2. Both the "Second peptides" and "Match between runs" options were also allowed. Following the analysis, the results were sorted according to several parameters. Proteins positive for at least either one of the "Reverse", "Only.identified.by.site" or "Potential.contaminant" categories were eliminated, as well as proteins identified from a single peptide.

2.9 Mass Spectrometry Data Analysis

The average peptide count data was filtered using the CRAPome repository [86] to remove common LC-MS/MS contaminants with a threshold score of 0.2. The residual proteins from the APEX2-PML data sets were then compared against the APEX2-NLS protein data sets using the default settings of the program SAINT express [87]. Proteins that met the SAINT score threshold of 0.2 were included. Dot plots of the resulting proteins with respect to treatment were made using ProHits-viz with a Bayesian false discovery rate threshold of 0.05 [88]. The proteins that passed both the SAINT score and CRAPome filters were pooled, and their interaction networks analyzed using STRING v11 [89].

2.10 siRNA Knock Down of MK2

Thirty-five mm dishes were seeded at 150,000 cells per and allowed to reach 65% confluency. Cells were transfected with siRNAs targeting human MK2 or a non-targeting control siRNA (Dharmacon Table 2.15**)** The siRNA transfection mixture was prepared by mixing 100 nM of siRNA with 10 µl of Lipofectamine-2000 in 400 µl DMEM and incubating for 30 minutes at 37 °C and 5% CO_2. The transfection mixture was added to dishes containing 1.5 ml of media and incubated overnight. Cells were harvested 48 h later.

2.11 Stimulation and Inhibition of p38 Signaling Cascade

To inhibit p38 or MK2, cells were pre-treated with 10 µM SB-203580 or PF-3644022 dissolved DMSO, respectively, for 20 min. To activate the p38 phosphorylation cascade, cells were treated with 0.5 µM anisomycin for 30 mins. Cells were then harvested for SDS-PAGE as described in 2.3 or fixed for immunofluorescence as described in 2.4.

2.12 Isolation of Biotinylated Proteins on Neutravidin-Sepharose

The procedure for this methods section was adapted from James et al. (2019). After cells were transfected with plasmids encoding APEX2 fusion proteins, incubated with biotin-phenol and pulsed with hydrogen peroxide as described in 2.2 and 2.7 respectively, cells were scraped in PBS and collected by centrifugation at 2,000 rpm for 5

min. The cell pellet was lysed in 1 ml of lysis buffer (50 mM Tris, pH 7.4, 5 mM Trolox, 0.5% (w/v) sodium deoxycholate, 150 mM NaCl, 0.1% (w/v) SDS, 1% (v/v) Triton X-100, 1 mM phenylmethanesulfonylfluoride (PMSF), 10 mM NaN_3, 10 mM sodium ascorbate, 1x protease inhibitor) for 5 min on ice then centrifuged for 10 min at 13,000 g at 4 °C.

The neutravidin beads were prepared by washing with lysis buffer twice before resuspension in a 1:1 ratio in lysis buffer. The cell lysates were incubated with 100 µl of neutravidin beads for 12 h at 4 °C on an orbital rotor. The beads were collected by centrifugation whereafter they were washed once with washing buffer 1 (50 mM HEPES, pH 7.4, 0.1% (w/v) sodium deoxycholate, 1% (v/v) Triton x-100, 500 mM NaCl, and 1 mM EDTA), once with washing buffer 2 (50 mM Tris, pH 8.0, 250 mM LiCl, 0.5% (v/v) Nonidet p-40, 0.5% (w/v) sodium deoxycholate, and 1 mM EDTA), and twice with washing buffer 3 (50 mM Tris, pH 7.4, 50 mM NaCl). Each washing step beads were incubated for 5 min at 4 °C on an orbital rotor and collected by centrifugation.

The proteins were eluted from Neutravidin bead pellet by incubation with 45 µl of SDS sample buffer (4% (w/v) SDS, 125 mM Tris, pH 6.8, 10% (v/v) glycerol, 0.02% (v/v) bromophenol blue, and 10% (v/v) β-mercaptoethanol) supplemented with 5 mM desthiobitoin for 5 min at 95 °C [90]. Protein samples were then be resolved by SDS-PAGE and immunoblotted to detect biotinylated proteins (see section 2.3).

2.13 LAPS Quantification

Twenty fields of cells were randomly selected on the DAPI channel for the control, and treatment cells. The number of experimental replicates is indicated in the figure descriptions. The images were then quantified by manual counting of the LAPS per nuclei.

2.14 Primers Used

Name	Sequence	Notes
APEX2 PML forward	5’gcatgctagccaccatgggaaagtctt3’	NheI
APEX2 PML/NLS reverse	5’ggtgtacagagcgtaatctggaacatcg3’	BsrGI
APEX2 NLS forward	5’gcggtacccaccatgggaaagtcttac3’	KpnI

2.15 siRNA Table

Name	Target sequence	Product number
Human siMK2#1	CGAAAUGGGCCAGUAUGAAU,	J-003516-11-0002
Human siMK2#2	GUUAUACACCGUACUAAUGU,	J-003516-12-0002
Human siMK2#3	GGCAUCAACGGCAAAGUUU,	J-003516-13-0002
Human siMK2#4	CCACCAGCCACAAACUCUUU	J-003516-14-0002
non-targeting control siRNA	UGGUUUACAUGUCGACUAA	D-00120614-05

Chapter 3: Results

3.1 APEX2-PML Localize to nLDs

To investigate the proteome of LAPS using APEX2 labelling, I constructed plasmids encoding APEX2-HA-PML isoform I and II. These plasmids were also engineered to have a C-terminal HA tag between APEX2 and PML to visualize their expression on LAPS by confocal microscopy when transiently transfected into U2OS cells. Both APEX2-HA-PML-1 (**Figure 3.1**) and APEX2-HA-PML-II (**Figure 3.2**) were seen on PML-NBs and on LAPS after inducing their formation with 500 μM oleate. Under oleate treated conditions the canonical ring structures with the HA tag are seen surrounding nLDs.

3.2 APEX2-PML Biotinylation Reaction on LAPS

Since the constructs were associating with LAPS, I tested whether APEX2-PML could biotinylate associated proteins. To accomplish this U2OS cells transiently expressing APEX2-PML were treated with or without biotin-phenol followed by addition of H_2O_2 to initiate the biotinylation reactions catalyzed by APEX2. The biotinylated proteins were visualized by immunofluorescence with an Alexa Fluor™ 488 conjugated to streptavidin.

As seen by immunofluorescence, when treated with both biotin-phenol and H_2O_2 the APEX2-HA-PML-I had an increase in streptavidin signal surrounding the HA-positive LAPS (**Figure 3.3**). This was also accompanied with diffuse background nuclear

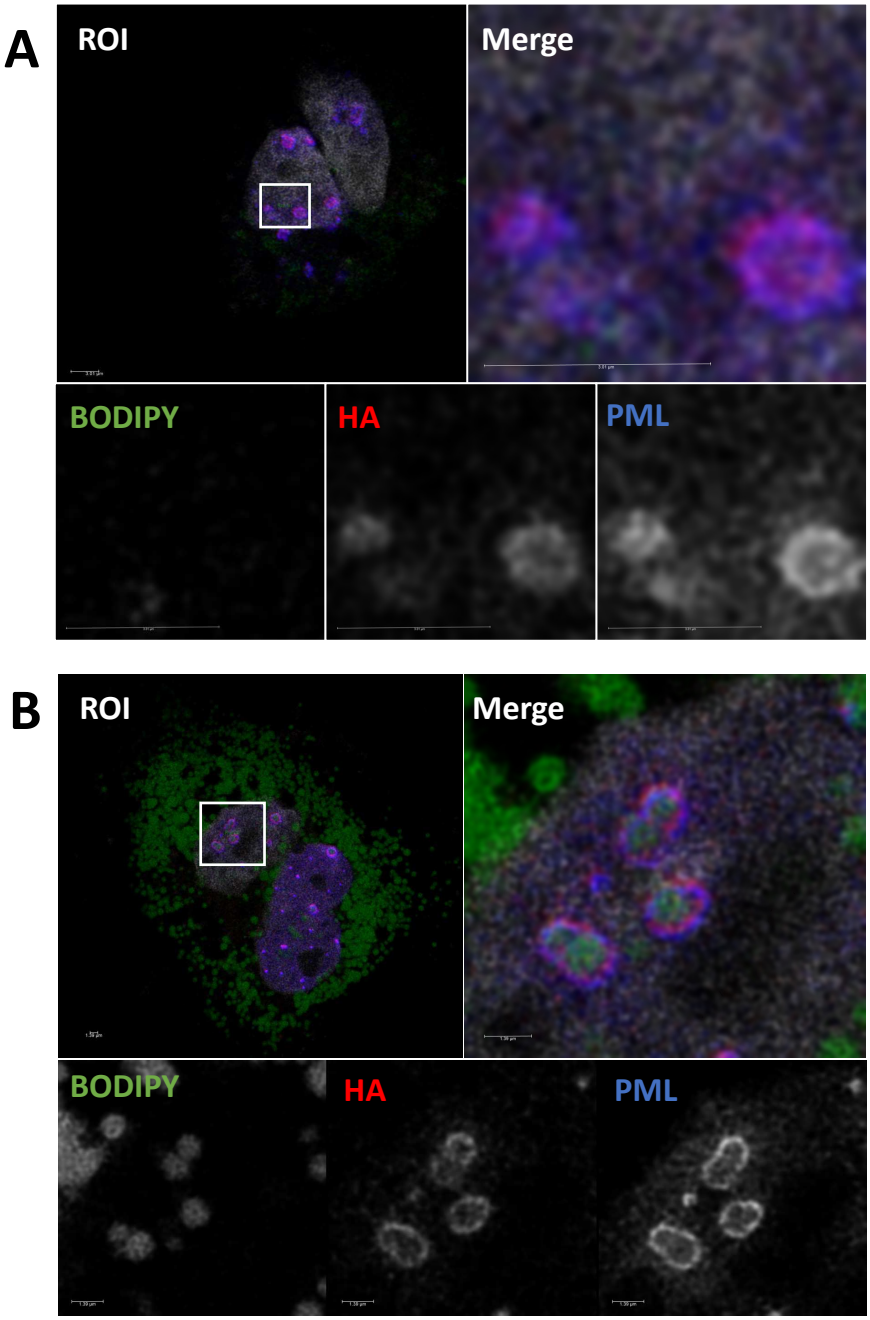

Figure 3.1. APEX2-HA-PML-I colocalize on LAPS with oleate treatment. (A) Untreated U2OS cells **(B)** 500 μM oleate treated U2OS cells. Cells were cultured in 35mm dishes with 1.0 mm coverslips. The media was replaced one day before with treatments before the cells were fixed and permeabilized as described in 2.4. The coverslips were probed with antibodies for BODIPY 493/503 1:1000 (green), anti-HA 1:1000 (red), and PML 1:2000 (blue). Nucleus was stained with Hoechst 1:1000 (grey). A Region Of Interest was cropped and the channels split into greyscale.

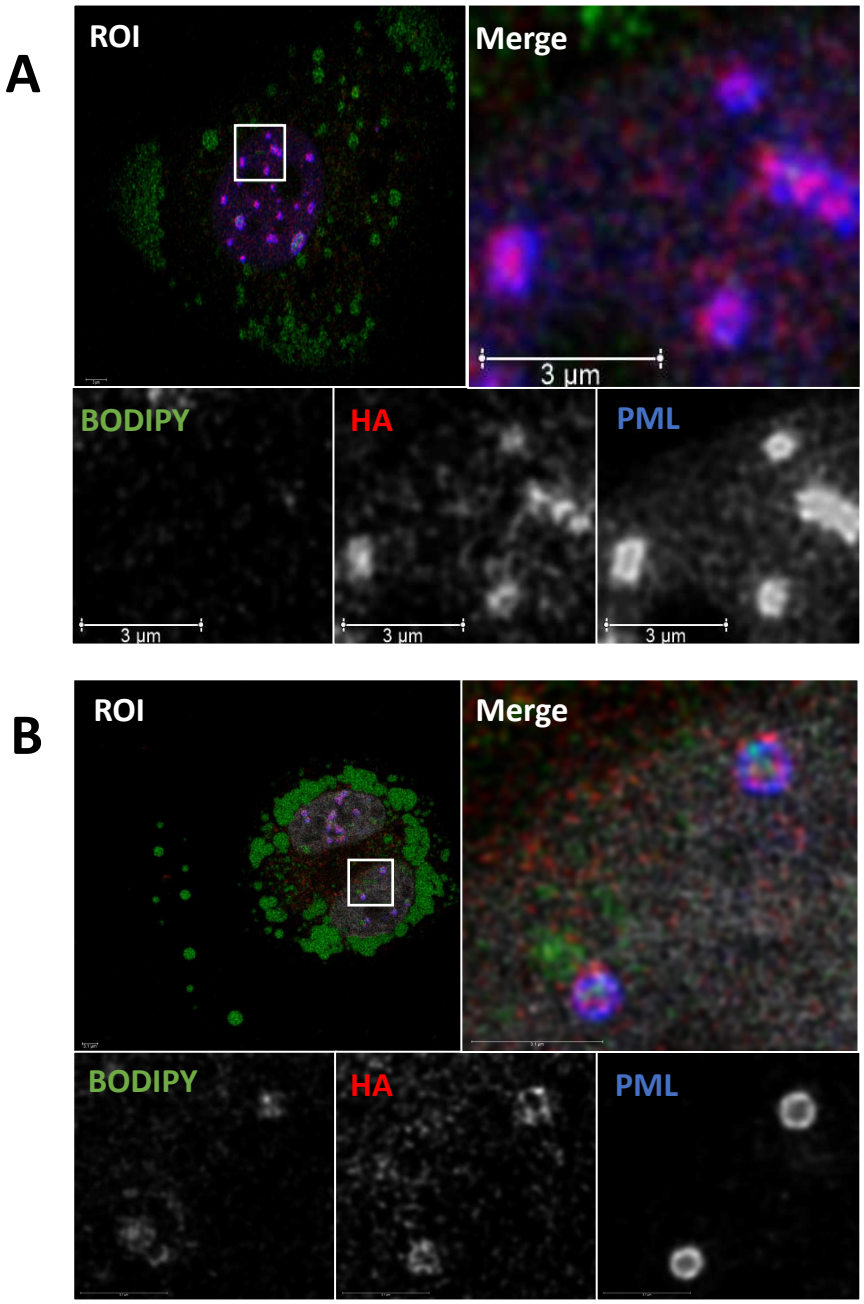

Figure 3.2. APEX2-HA-PML-II colocalize on LAPS with oleate treatment. (A) Untreated U2OS cells **(B)** 500 µM oleate treated U2OS cells. Cells were cultured in 35mm dishes with 1.0 mm coverslips. The media was replaced one day before with treatments before the cells were fixed and permeabilized as described in 2.4. The coverslips were probed with antibodies for BODIPY 493/503 1:1000 (green), anti-HA 1:1000 (red), and PML 1:2000 (blue). Nucleus was stained with Hoechst 1:1000 (grey). A Region Of Interest was cropped and the channels split into greyscale.

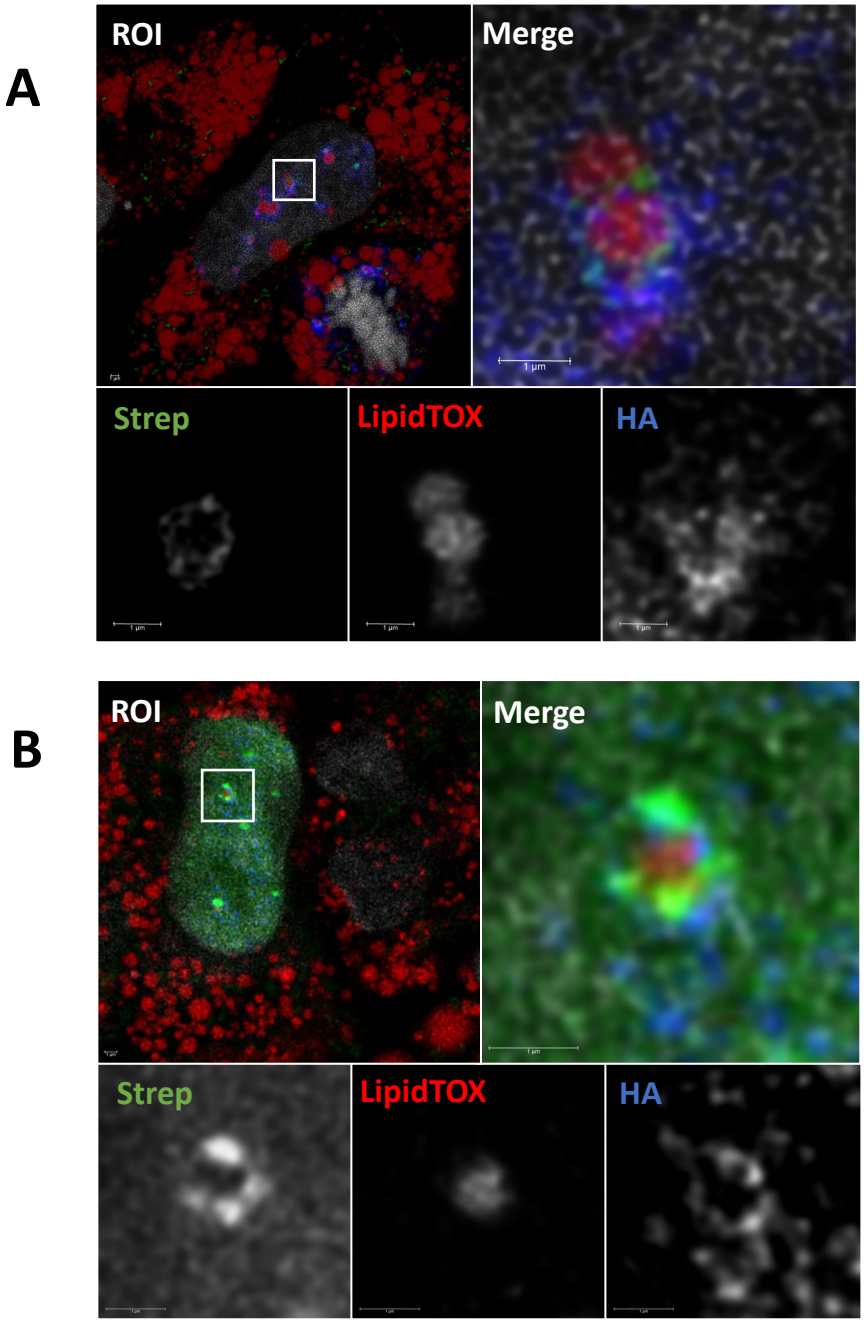

Figure 3.3. APEX2-HA-PML-I biotinylate around LAPS. (A) - Biotin phenol, + H_2O_2 U2OS cells **(B)** + Biotin phenol, + H_2O_2 U2OS cells. Cells were cultured in 35mm dishes with 1.0 mm coverslips. The media was replaced one day before with treatments before the cells were fixed and permeabilized as described in 2.4 . The coverslips were probed with antibodies for streptavidin-488 1:1000 (green), LipidTOX neutral red 1:1000 (red) anti-HA 1:1000 (blue). Nucleus was stained with Hoechst 1:1000 (grey). A Region Of Interest was cropped and the channels split into greyscale.

streptavidin signal indicative of proteins within the nucleoplasm being labelled when they came into proximity of APEX2-HA-PML-I. This is contrasted by the cells that were not treated with biotin-phenol that had no background nuclear streptavidin signal and little to no residual signal around the APEX2-HA-PML-I construct.

Similarly, the APEX2-HA-PML-II construct was also validated to have streptavidin signal around HA-positive LAPS with diffuse nuclear staining when treated with both biotin phenol and H_2O_2, while having minimal streptavidin signal around the construct when untreated (**Figure 3.4**).

3.3 APEX2-NLS Nuclear Localization and Biotinylation

To control for background biotinylation that was occurring throughout the nucleus, APEX2-HA-NLS was created. This construct was validated in a similar manner to APEX2-HA-PML described above. When U2OS cells were transiently transfected and then treated with biotin-phenol and H_2O_2 there was non-discriminant streptavidin signal throughout the nucleus of the cell when both reagents where present (**Figure 3.5**). Untreated cells had no streptavidin signal in the nucleus. The HA tag was also expressed in nucleus of transfected cells under both conditions, indicating that the APEX2-NLS constructs were functional.

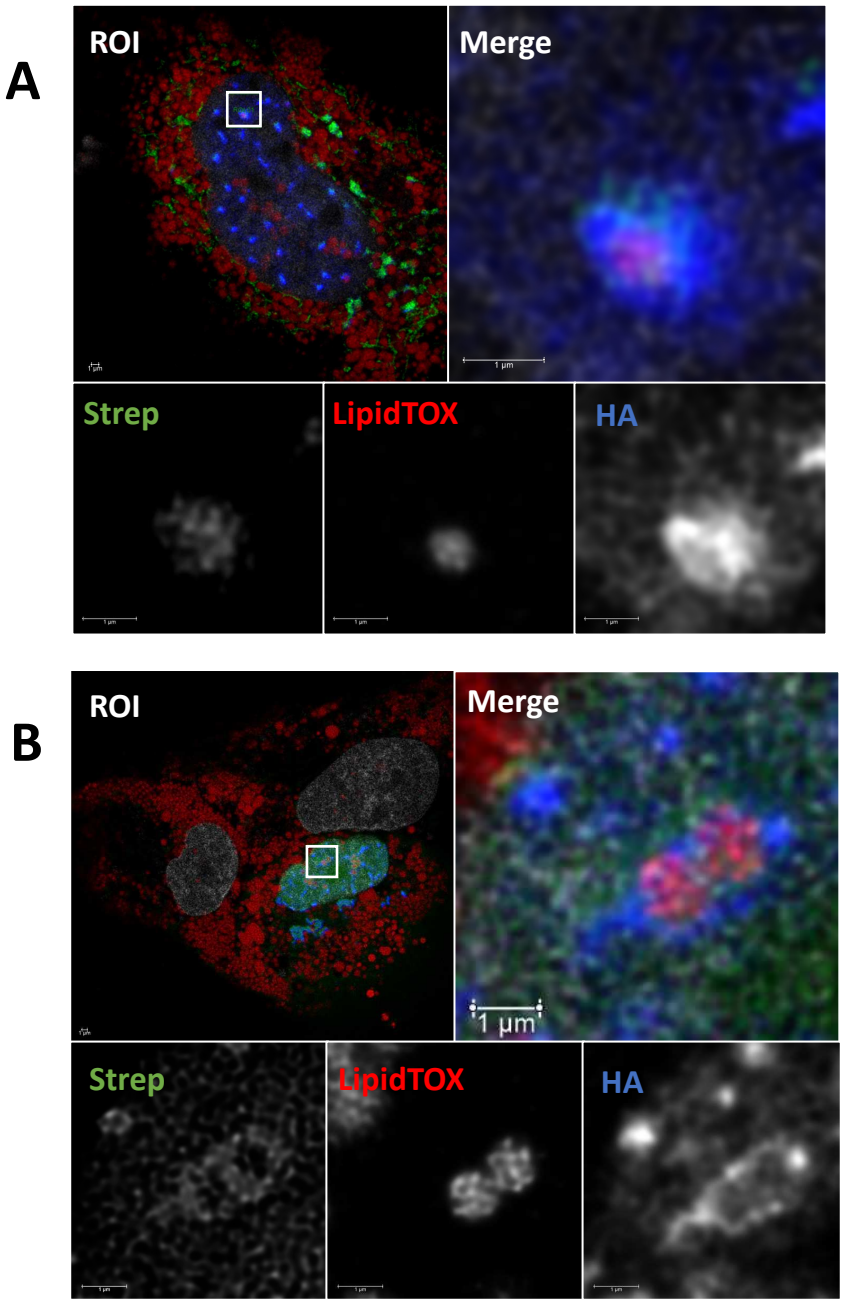

Figure 3.4. APEX2-HA-PML-II biotinylate around LAPS. (A) - Biotin phenol, + H_2O_2 U2OS cells **(B)** + Biotin phenol, + H_2O_2 U2OS cells. Cells were cultured in 35mm dishes with 1.0 mm coverslips. The media was replaced one day before with treatments before the cells were fixed and permeabilized as described in 2.4. The coverslips were probed with antibodies for streptavidin-488 1:1000 (green), LipidTOX neutral red 1:1000 (red) anti-HA 1:1000 (blue). Nucleus was stained with Hoechst 1:1000 (grey). A Region Of Interest was cropped and the channels split into greyscale. .

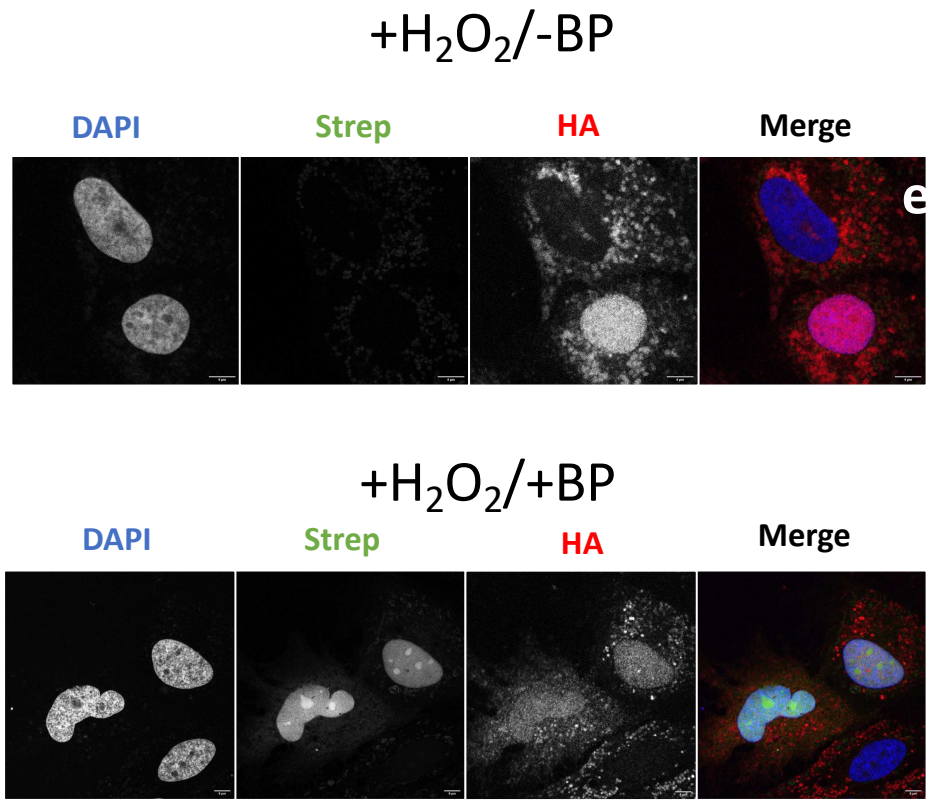

Figure 3.5 APEX2-HA-NLS localize and biotinylate the nucleus. U2OS cells were cultured in 35mm dishes with 1.0 mm coverslips. The media was replaced one day with 500 μM oleate before the cells were pulsed with +/- biotin-phenol and H_2O_2 then fixed and permeabilized as described in 2.4. The coverslips were probed with antibodies for streptavidin-488 1:1000 (green), and anti-HA 1:1000 (red). Nucleus was stained with Hoechst 1:1000 (grey).

3.4 LC-MS/MS Analysis

Since the APEX2-PML constructs were both localizing as expected and able to biotinylate nuclear proteins, I proceeded with the labelling experiments that would be sent for LC-MS/MS analysis by our collaborators at Sherbrook University. Duplicate sets of U2OS cells expressing APEX2-HA-PML-I, APEX2-HA-PML-II, or APEX2-HA-NLS were treated with or without 500 μM oleate for 24 hr. These cells were treated with both biotin-phenol and H_2O_2 to initiate the biotinylation reaction. Cells were lysed, separated by gel electrophoresis, and probed with an HA antibody and streptavidin conjugated fluor to determine that the cell pellets were expressing the constructs and that biotinylation occurred (**Figure 3.6**). The major protein bands for the APEX constructs can be seen in the HA antibody signal. APEX2 is a 27 kDA protein. With the additions of the HA tag and the NLS, we see the associated band just slightly larger than 31 kDa for APEX2-HA-NLS. Likewise, for the APEX2-HA-PML constructs, both PML isoforms have a mass of about 97 kDa. When conjugated to APEX2 we see the resulting fusion protein mass at just above 125 kDa. The other smaller HA bands seen are most likely degradation products of the fusion protein. These major APEX2-HA-PML protein bands are also shown to have associated streptavidin signal indicating self biotinylation. This blot demonstrates that the cell pellets sent for LC-MS/MS analysis were expressing the APEX2 constructs and that the biotinylation reaction occurred.

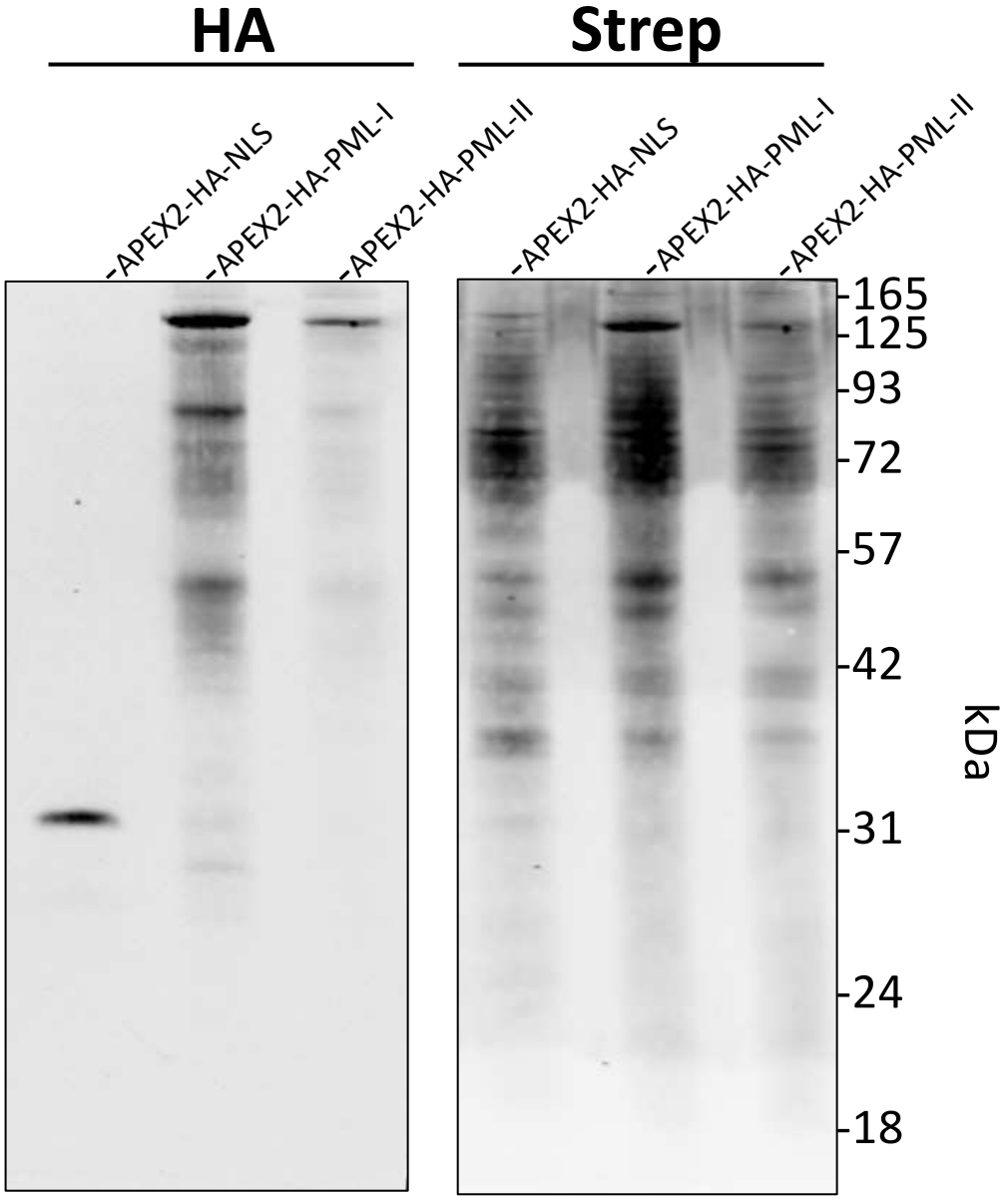

Figure 3.6 Anti-HA and Streptavidin conjugated fluor confirms APEX2 constructs expression and biotinylation activity in cells sent for LC-MS/MS. Lysates of aliquots of cells prepared for LC-MS/MS were resolved by SDS-PAGE and transferred to nitrocellulose. Immunoblotted with anti-HA (1:1000) and streptavidin conjugated fluors (1:1000).

3.5 PML Interactome

The biotinylated proteins were purified by a streptavidin pull-down and analysed using LC-MS/MS**.** High confidence interactors were selected by using the SAINT score analysis for both PML-I and II using APEX2-NLS as the background control. Across both PML isoforms, 66 interactors were identified for both PML-NB and LAPS. The interactors were then sorted into a dot plot to illustrate the isoform specific interactions for both LAPS and PML-NBs (**Figure 3.7**). More high confidence interactors were found to interact with LAPS in comparison to the PML-NBs for both of PML isoforms. Further the quality and quantity of the interactors was much higher for APEX2-HA-PML-I in contrast to APEX2-HA-PML-II.

All the proteins that were found to be high confidence interactors with PML isoforms in the presence and absence of oleate were pooled and analysed using the STRING network (**Figure 3.8**). The network diagram shows some highly interconnected clusters of endosomal sorting complexes required for transport (ESCRT) proteins such as TSG101, STAM and STAM2. Another cluster of SEC family proteins such as SEC23B, SEC24A, SEC24B, and SEC23IP were identified. Referencing this network of proteins back to the dot plot indicates that this interaction is occurring for both LAPS and PML-NBs given the plethora of proteins from these families found under all conditions.

One of the proteins found to be an interactor for PML I and II in oleate-treated cells was the kinase MAPKAPK2 (MK2) encoded by the *MAPKAPK2* gene. When cells are stimulated with inflammatory cytokines, the protein kinase p38 phosphorylates MK2. This results in MK2 activation and the phosphorylation of other protein targets such as

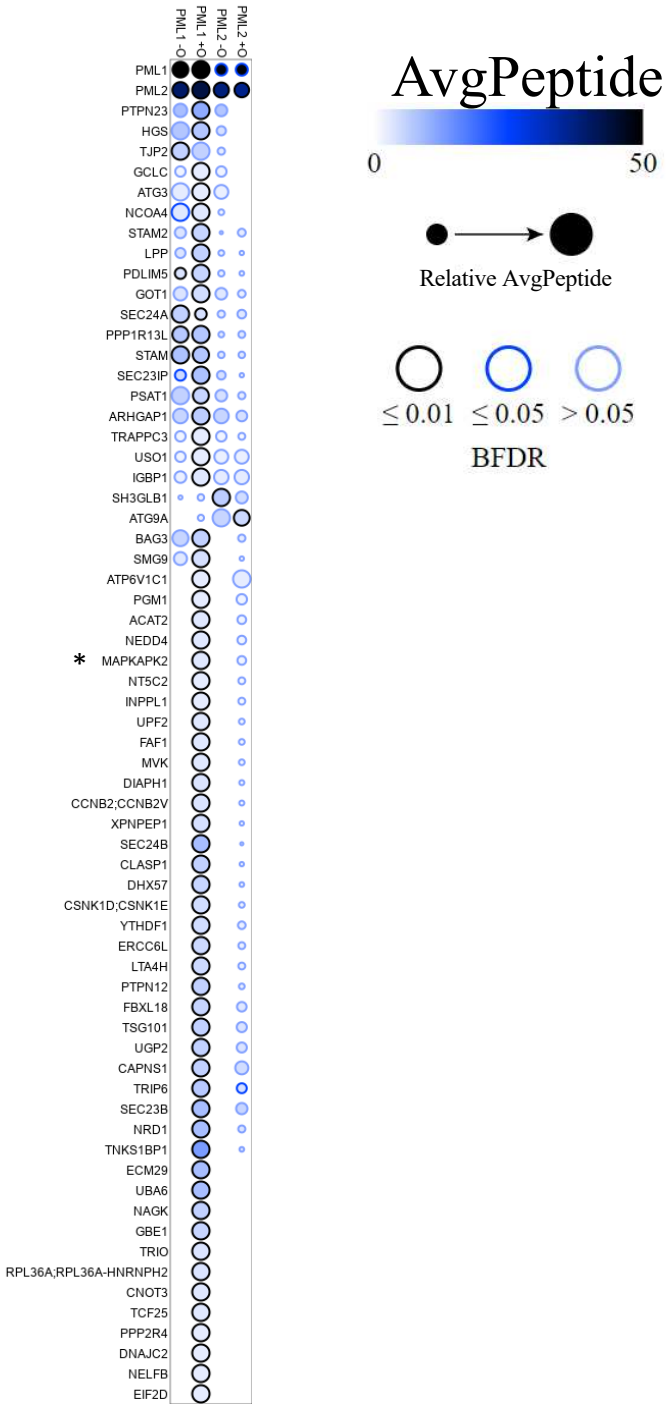

Figure 3.7 APEX2-PML interactome dot plot for isoform specific interactions. Average peptide count data filtered using the CRAPome repository with a threshold score of 0.2 and SAINTexpress with a threshold of 0.2. The dotplot was generated using ProHits-vis and filtered using a Bayesian false discovery rate of 0.05. Asterix highlights the MAPKAPK2 protein encoded by *MAPKAPK2* gene.

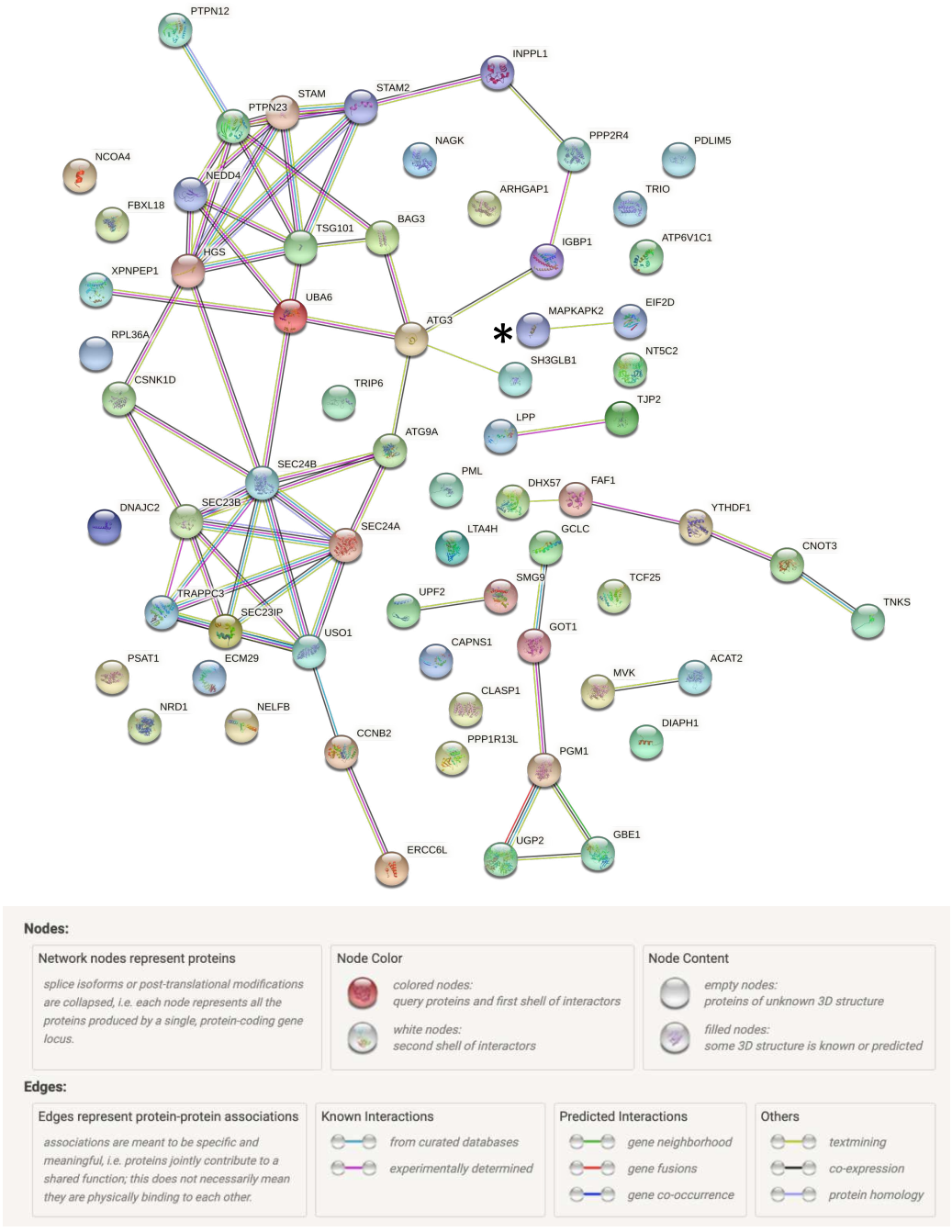

Figure 3.8 APEX2-PML interactome STRING network interactions. Average peptide count data filtered using the CRAPome repository with a threshold score of 0.2 and SAINTexpress with a threshold of 0.2. All identified proteins across both isoforms and treatments were pooled and analysed using STRING V11. Asterix highlights the MAPKAPK2 protein encoded by *MAPKAPK2* gene.

heat shock protein 27 (HSP27) and Receptor-interacting serine/threonine-protein kinase 1 (RIPK1) [91, 92]. Another function of MK2 is to increase the mRNA stability of tumor necrosis factor (TNF) through the phosphorylation of factors interacting with the 3'AU-rich elements (AREs) allowing for sustained cytokine production [93]. Structurally, MK2 contains a N-terminal proline rich region, followed by the kinase domain and lastly a C-terminal regulatory domain. At the C-terminal region the two main isoforms of MK2 differ. The isoform MK2-I is truncated and does not contain an NLS, whereas the full length MK2-II has an NLS [94]. Though this kinase was not connected to any of the major STRING networks, it is of particular interest due to a recent paper that demonstrated MK2 interactions with PML-NBs inhibits the p38-MAPK phosphorylation, thereby promoting necroptosis and apoptosis [95]. The protein MK2 was pursued further to characterize its interaction with PML and LAPS.

3.6 MK2 Associates with PML

To validate the interactome, I sought to determine if MK2 interacted with PML. To accomplish this, U2OS cells (**Figure 3.9**) and Huh7 cells (**Figure 3.10**) transiently expressing MK2-II-FLAG and treated with oleate were visualized by IF. The overexpressed MK2-II-FLAG was diffuse throughout the cell but concentrated in the nucleus. Given the nature of overexpressing protein it is expected that some of the normally nuclear localized protein escapes to the cytoplasm. Near the top of the cell, MK2-II-FLAG formed ring structures around LAPS. These interactions were accompanied by voids in the nuclear DAPI staining. This interaction is seen most clearly

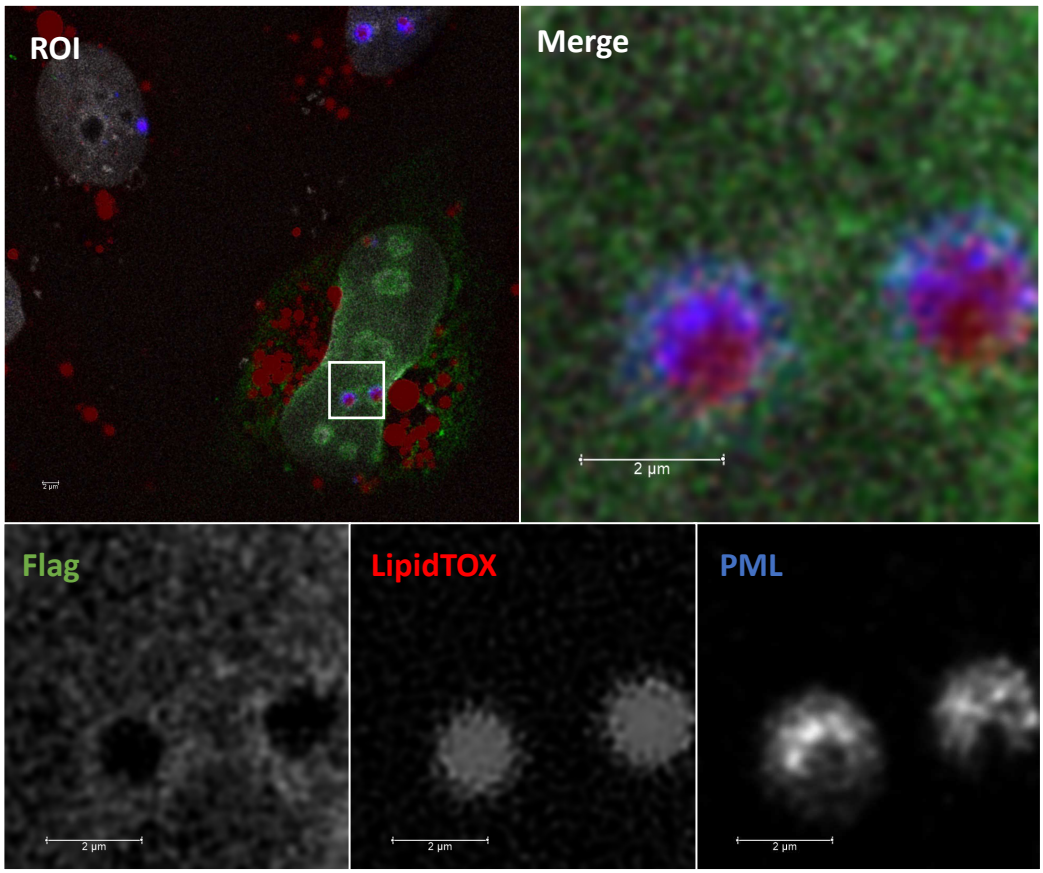

Figure 3.9. Overexpressed MK2-II associates with LAPS in U2OS cells. U2OS cells were cultured in 35mm dishes with 1.0 mm coverslips. The cells were transfected with pMK2-II-Flag. The media was replaced one day with 500 µM oleate before being fixed and permeabilized as described in 2.4. The coverslips were probed with antibodies for anti-flag 1:1000(green), LipidTOX neutral red 1:1000 (red) anti-PML 1:2000 (blue). Nucleus was stained with Hoechst 1:1000 (grey). A Region Of Interest was cropped and the channels split into greyscale.

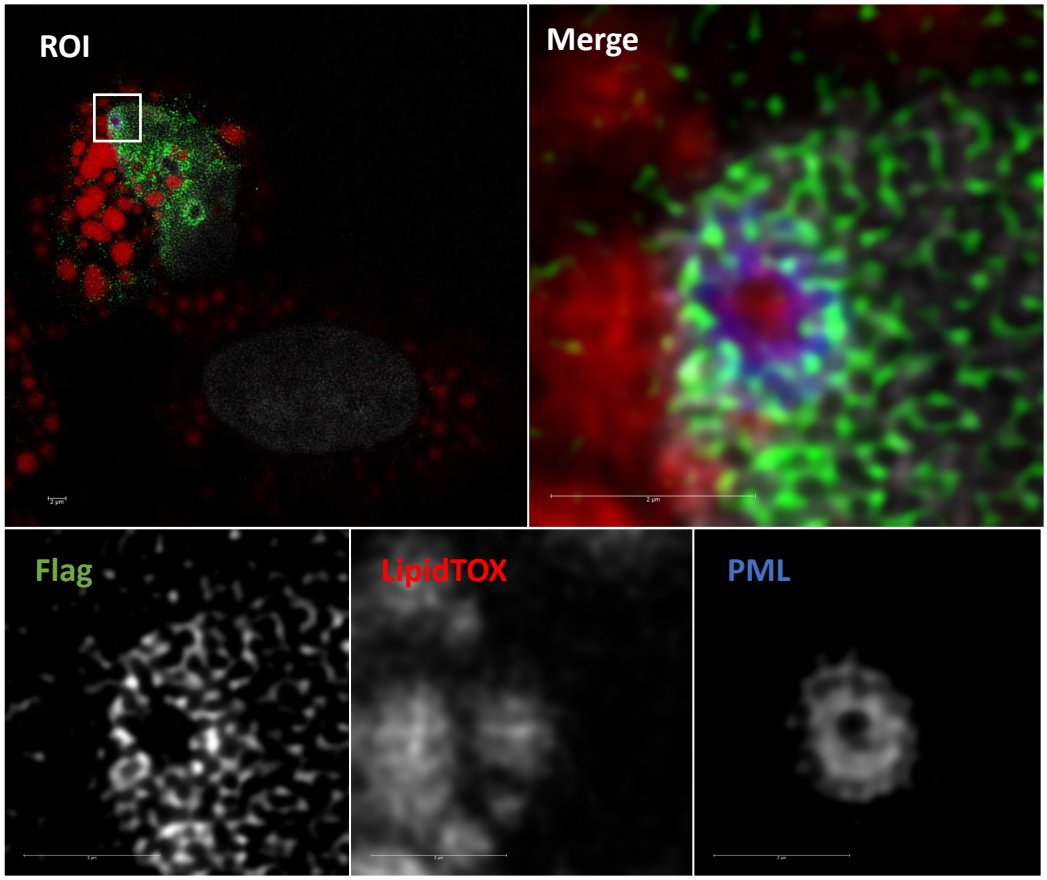

Figure 3.10 Overexpressed MK2-II associates with LAPS in Huh7 cells. HUh7 cells were cultured in 35mm dishes with 1.0 mm coverslips. The cells were transfected with pMK2-II-Flag. The media was replaced one day with 500 μM oleate before being fixed and permeabilized as described in 2.4. The coverslips were probed with antibodies for anti-flag 1:1000(green), LipidTOX neutral red 1:1000 (red) anti-PML 1:2000 (blue). Nucleus was stained with Hoechst 1:1000 (grey). A Region Of Interest was cropped and the channels split into greyscale.

with the 3D reconstruction of a U2OS z-stack, which illustrates the diffuse MK2-II-FLAG signal that concentrates at the top of the nuclear lipid droplet (**Figure 3.11**). Similarly, MK2-I-FLAG was expressed in U2OS cells. The overexpressed protein was observed to interact with both LAPS and PML-NBs (**Figure 3.12**). Given that this interaction was verified by IF and the APEX2 interactome, I investigated if MK2 was forming an isoform specific interaction with PML. To accomplish this, GFP-tagged PML-I, PML-II and PML-IV were transiently expressed into PML knockout U2OS cells (**Figure 3.13**). Since PML-IV has the same exon structure as PML-I except for missing the last exon 9, it was used as a control to differentiate between the PML-I and PML-II. MK2 was found to associate with the overexpressed GFP-tagged PML only in the cells overexpressing PML-I. This indicates that PML exon 9 is necessary for the interaction between PML and MK2.

3.7 The Effect of p38 Inhibition on LAPS

Since MK2 is a part of the p38 kinase cascade and MK2 is interacting with LAPS, I sought to investigate how the LAPS were altering the phosphorylation and expression of proteins in the p38 cascade. To accomplish this, a baseline analysis of expression and phosphorylation of the proteins involved in the p38 cascade was first required. To induce p38 cascade signalling, U2OS cells were treated with the drug anisomycin, a well characterized stimulator of the p38 signalling cascade. Additionally, the p38 ATP-competitive inhibitor drug SB-203580 (SB), and MK2 ATP-competitive inhibitor PF-3644022 (PF) were utilized. They were used to observe how blocking the kinase

A

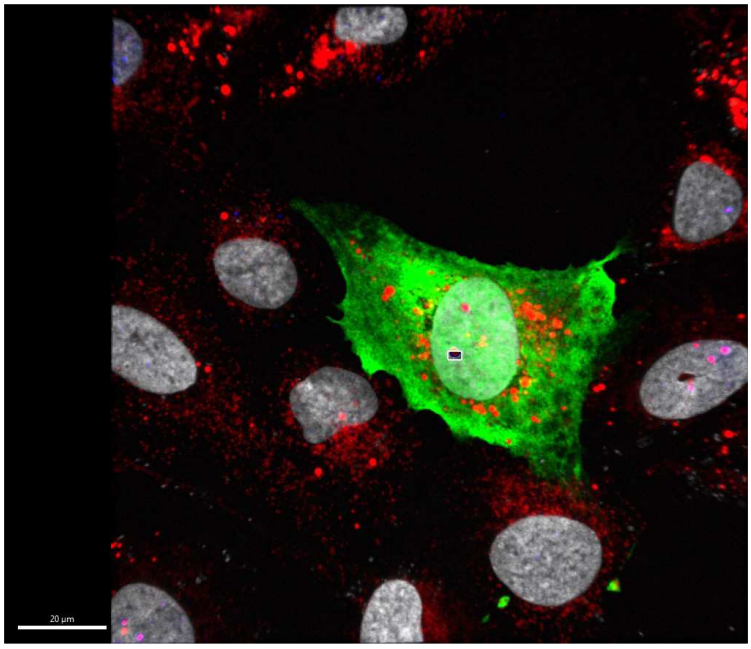

B

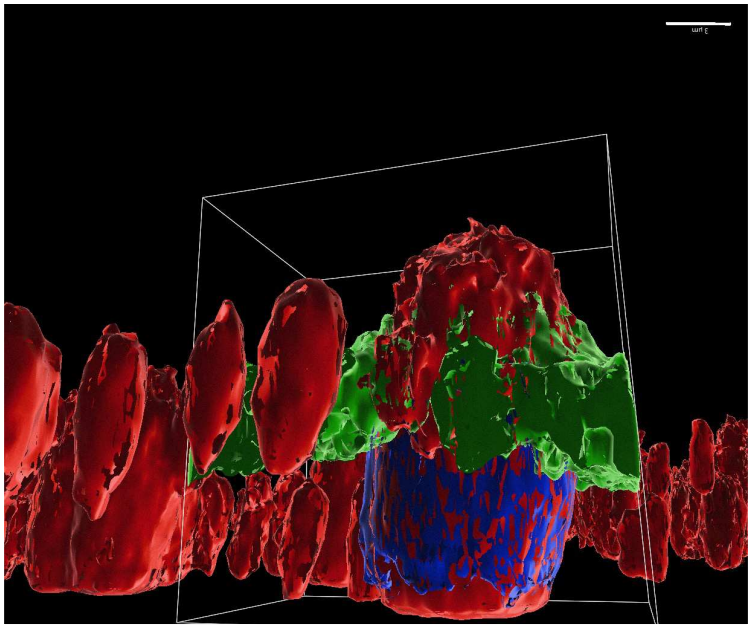

Figure 3.11. Overexpressed MK2 associates with LAPS 3D reconstruction. U2OS cells were cultured in 35mm dishes with 1.0 mm coverslips. The cells were transfected with MK2-II-Flag. The media was replaced one day with 500 µM oleate before being fixed permeabilized as described in 2.4. The coverslips were probed with antibodies for anti-flag 1:1000 (green), LipidTOX neutral red 1:1000 (red) anti-PML 1:2000 (blue). Nucleus was stained with Hoechst 1:1000 (grey). A Region Of Interest was cropped and rendered using Imaris.

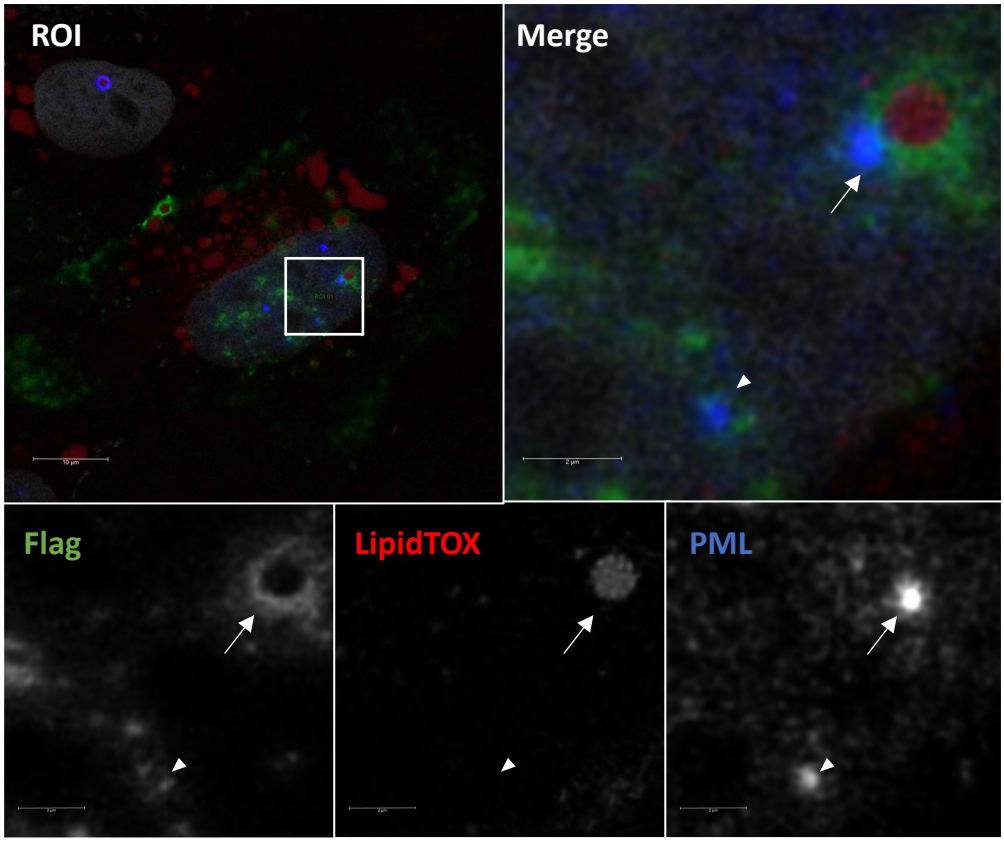

Figure 3.12. Overexpressed MK2-I associates with LAPS and PML-NBs. U2OS cells were cultured in 35mm dishes with 1.0 mm coverslips. The cells were transfected with pMK2-I-Flag The media was replaced one day with 500 μM oleate before being fixed and permeabilized as described in 2.4. The coverslips were probed with antibodies for anti-flag 1:1000 (green), LipidTOX neutral red 1:1000 (red) anti-PML 1:2000 (blue). Nucleus was stained with Hoechst 1:1000 (grey). A Region Of Interest was cropped and the channels split into greyscale. The arrows and chevron in magnified panels MK2 associating with LAPS and a PML-NB respectively.

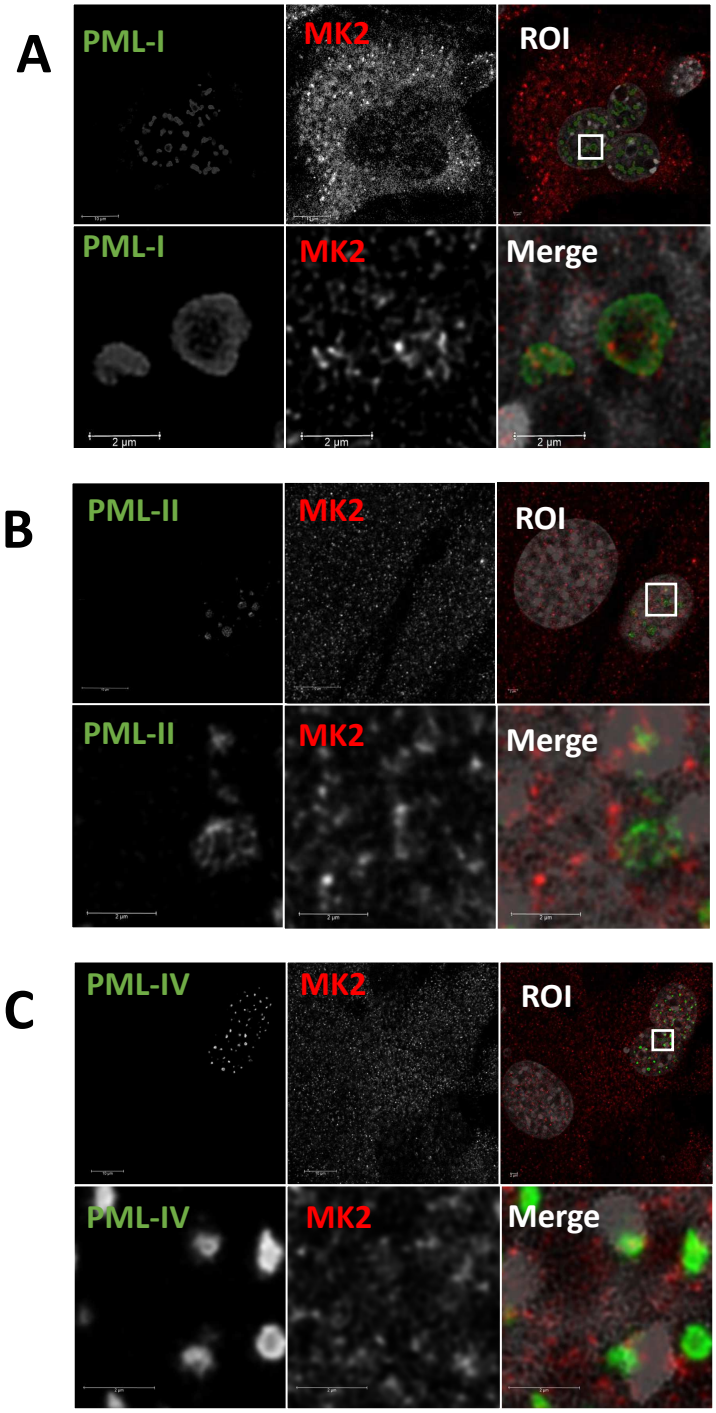

Figure 3.13. MK2 associates exclusively with PML-I. (A)U2OS cells transfected with pGFP-PML-I. **(B)**U2OS cells transfected with pGFP-PML-II. **(C)**U2OS cells transfected with pGFP-PML-IV. Cells were cultured in 35mm dishes with 1.0 mm coverslips. The media was replaced with 500 µM oleate one day before being fixed and permeabilized as described in 2.4. The coverslips were probed with antibodies for anti-MK2 1:200 (red). Nucleus was stained with Hoechst 1:1000 (grey). A Region Of Interest was cropped and the channels split into greyscale.

activities at these two enzymes effected downstream phosphorylation. Cells were treated with or without anisomycin, or anisomycin with either one of the inhibitors (**Figure 3.14**). There was an increasing in protein mass in both p38 protein and p38 pT180/Y182 for the anisomycin, anisomycin + SB, and the anisomycin + PF. This is indicative of p38 phosphorylation, which activates the p38 kinase activity. In the control cells and cells treated with anisomycin + PF inhibitor, the MK2 protein band moved from a doublet to a singlet corresponding to the increased signal for MK2 pT334. MK2 is phosphorylated directly by p38 at serine 334, which leads to its activation and phosphorylation of other proteins such as HSP27 [96]. Lastly, HSP27 had consistent protein levels across treatments, but had an increased pS82 signal in the anisomycin treated cells. Phosphorylation of serine 82 occurs through direct phosphorylation of MK2. These data show that the p38 signalling cascade is intact in U2OS cells treated with anisomycin, as well as the effectiveness of the p38 and MK2 inhibitors.

Given that I was able to inhibit p38 and MK2 phosphorylation using the SB and PF inhibitors, respectively, the effect of these drugs on LAPS formation was investigated. To accomplish this U2OS cells were pretreated with the two drugs before treatment with 500 μM oleate for 24 h (**Figure 3.15**). There was no statistical difference between the LAPS/cell for control verses SB treated cells. In contrast, PF treated cells had a statistically significant increase in the LAPS/cell. This indicates that MK2 enzymatic activity plays an important role in the formation of LAPS, and potentially in regulating lipid metabolism.

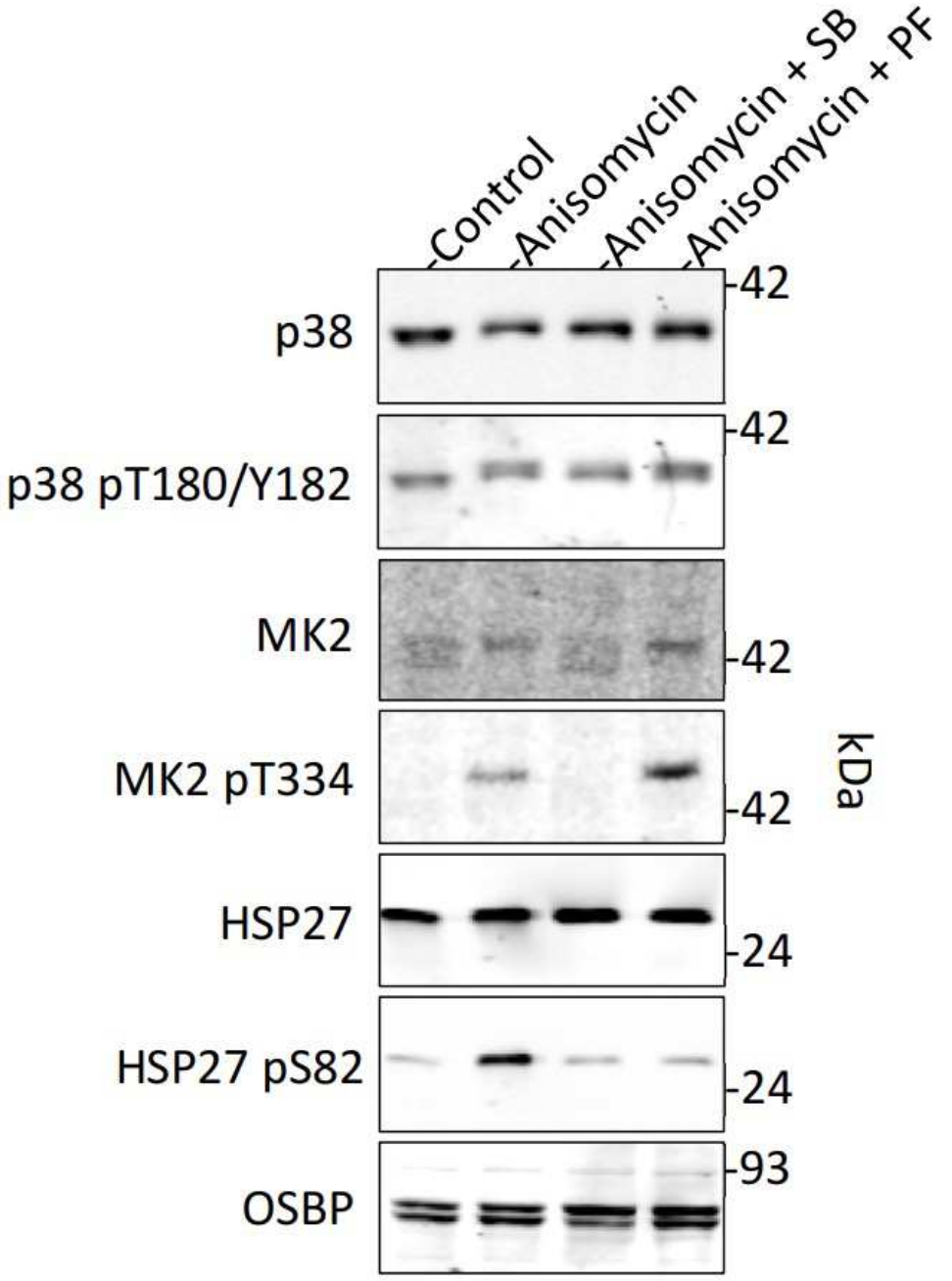

Figure 3.14 Inhibition of p38 kinase activity with SB-203580 or MK2 kinase activity with PF-3644022 treatment in anisomycin stimulated cells. U2OS cells were pretreated for 20 mins with 10 μM SB-203580 or PF-3644022 followed by 0.5 μM anisomycin for 30 mins,. Lysates cells were resolved by SDS-PAGE and transferred to nitrocellulose. Immunoblotted with anti-p38 (1:1000), anti-p38 pT180/Y182 (1:1000), anti-MK2 (1:1000), anti-MK2 pT334 (1:1000), anti-HSP27 (1;1000), anti-HSP27 pS82 (1:1000) or anti-OSBP (1:10000).

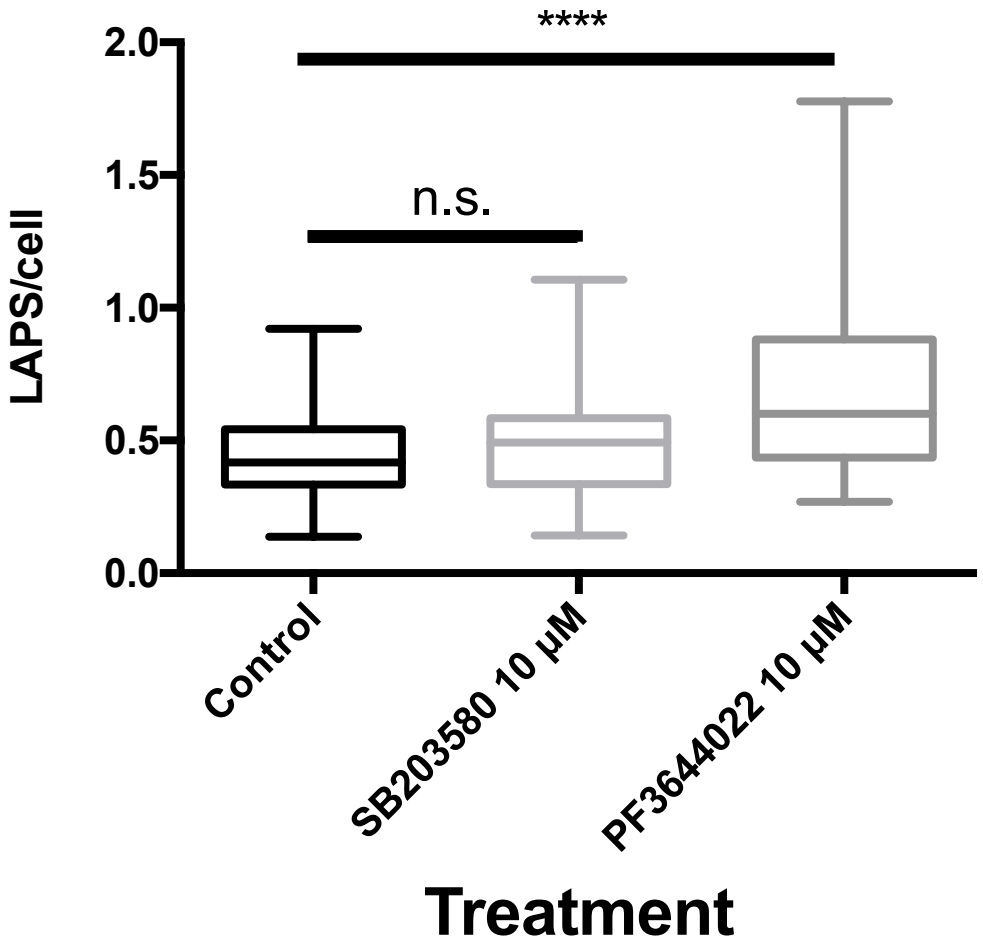

Figure 3.15 Inhibition of MK2 with PF-3644022 significantly increases the number of LAPS/cell. U2OS cells were pretreated for 20 mins with 10 µM SB-203580 or PF-3644022 before being treated with 500 µM oleate. Twenty fields of cells per experiment for each treatment were quantified manually. The results from 3 experiments were pooled. Total cells quantified were 1805, 1537, and 1595 for the control, SB, and PF treated cells respectively.

To compliment the drug treatment experiments, siRNA was used to knockdown the expression of MK2. Four different siRNAs targeting MK2 were screened (**Figure 3.16**). In comparison to the siRNA control cells, siMK2 #4 showed the highest knockdown efficiency of approximately 80 % whereas siMK2 #1, siMK2 #2, and siMK2 #3 showed a slightly lower knockdown efficiency of 60.5 %, 65 %, and 65.5 %, respectively. With the knockdown efficiency of the siRNA determined, U2OS cells were transfected with the MK2 targeting siRNA, before being treated with 500 μM oleate for 24 h (**Figure 3.17**). There was no statistical difference in the LAPS/cell of siMK2 treated cells in comparison to the control cells. This data indicates that partial knock down of MK2 is insufficient to achieve similar results of the MK2 kinase inhibition via drug treatment.

3.8 Role of LAPS on p38 Cascade

A recent paper indicated that PML promoted RIPK1 pS166 dependant necroptosis by sequestering both MK2 and p38. MK2 directly phosphorylates RIPK1 at the serine 321 preventing RIPK1 autophosphorylation at serine 166 [95]. However, this paper did not investigate the role of LAPS on the pathway by the addition of oleate. With the previous data showing how the p38 kinase cascade is stimulated with anisomycin, I proceeded to investigate if LAPS were affecting RIPK1 phosphorylation through the p38 signalling pathway. To do this U2OS and U2OS PML KO cells were treated with both +/- anisomycin and +/- oleate (**Figure 3.18**). In U2OS cells, there was no difference in protein expression or phosphorylation of p38, MK2, HSP27, and RIPK1 in cells treated

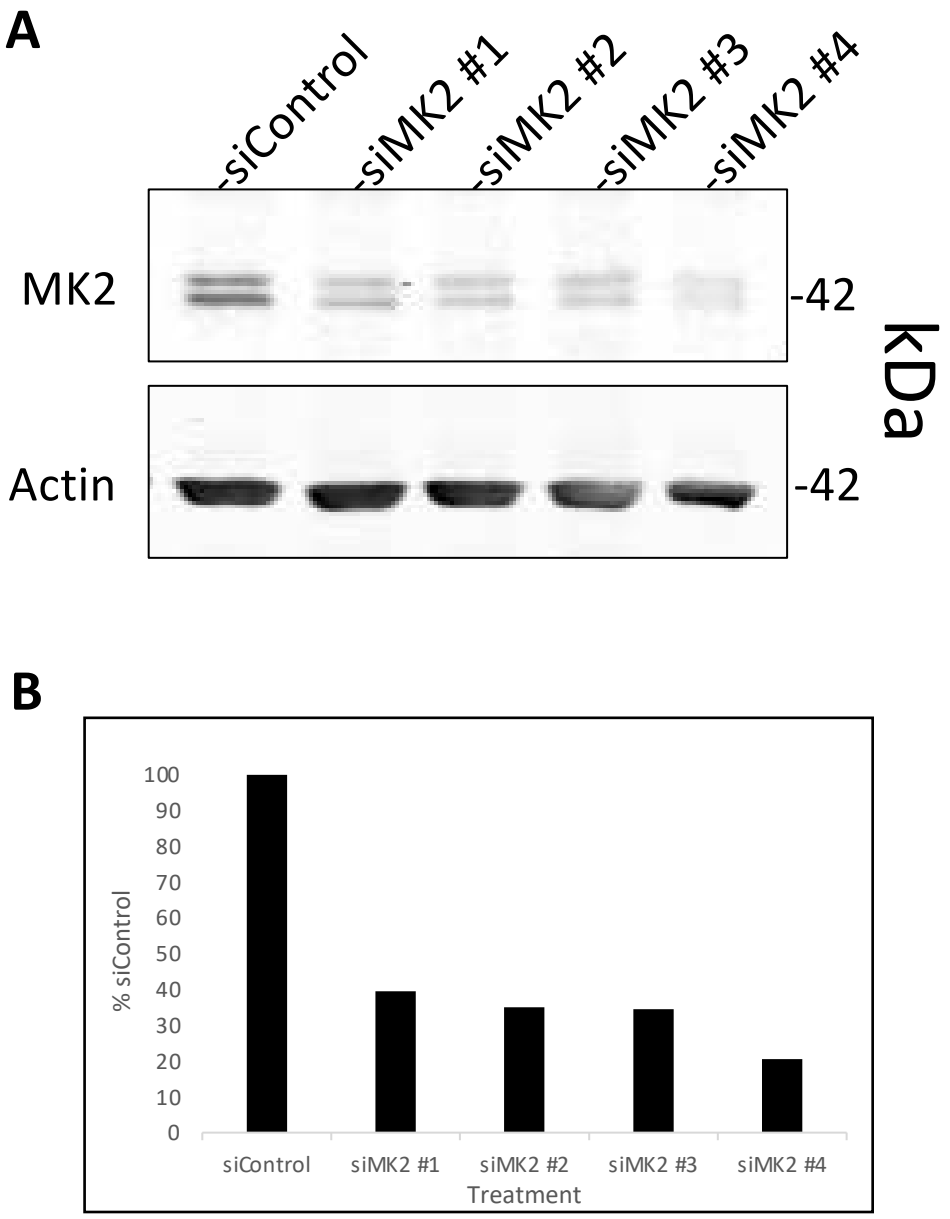

Figure 3.16 siRNA knock down of MK2 and quantification of reduction. (A) U2OS cells were treated with either a non-targeting siRNA or an siRNA targeting MK2. Lysates cells were resolved by SDS-PAGE and was transferred to nitrocellulose. Immunoblotted with anti-MK2 (1:1000), anti-actin(1:20000).**(B)** The quantification of the signal was the integrated intensity of the MK2/actin for each treatment divided by of the integrated intensity of MK2/actin of the non-targeting siControl treatment from one experiment.

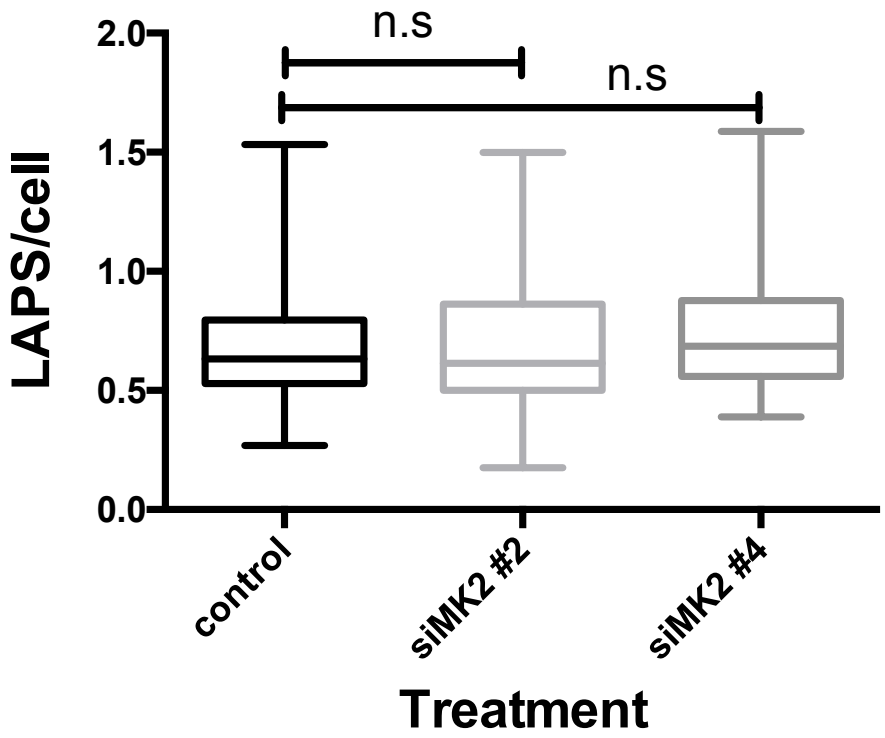

Figure 3.17 siRNA targeting MK2 has no effect on LAPS/cell. U2OS cells were either transfected with a non-targeting siRNA or an siRNA targeting MK2. The media was changed the next day and the cells were treated with 500 μM oleate for 24 h. Twenty fields of cells for each treatment were quantified manually. The results were pooled from 3 experiments for control and 2 experiments for siMK2 #2 and #4. Total cells quantified were 1419, 837, and 857 for the control, siMK2#2, siMK2#4 treated cells respectively.

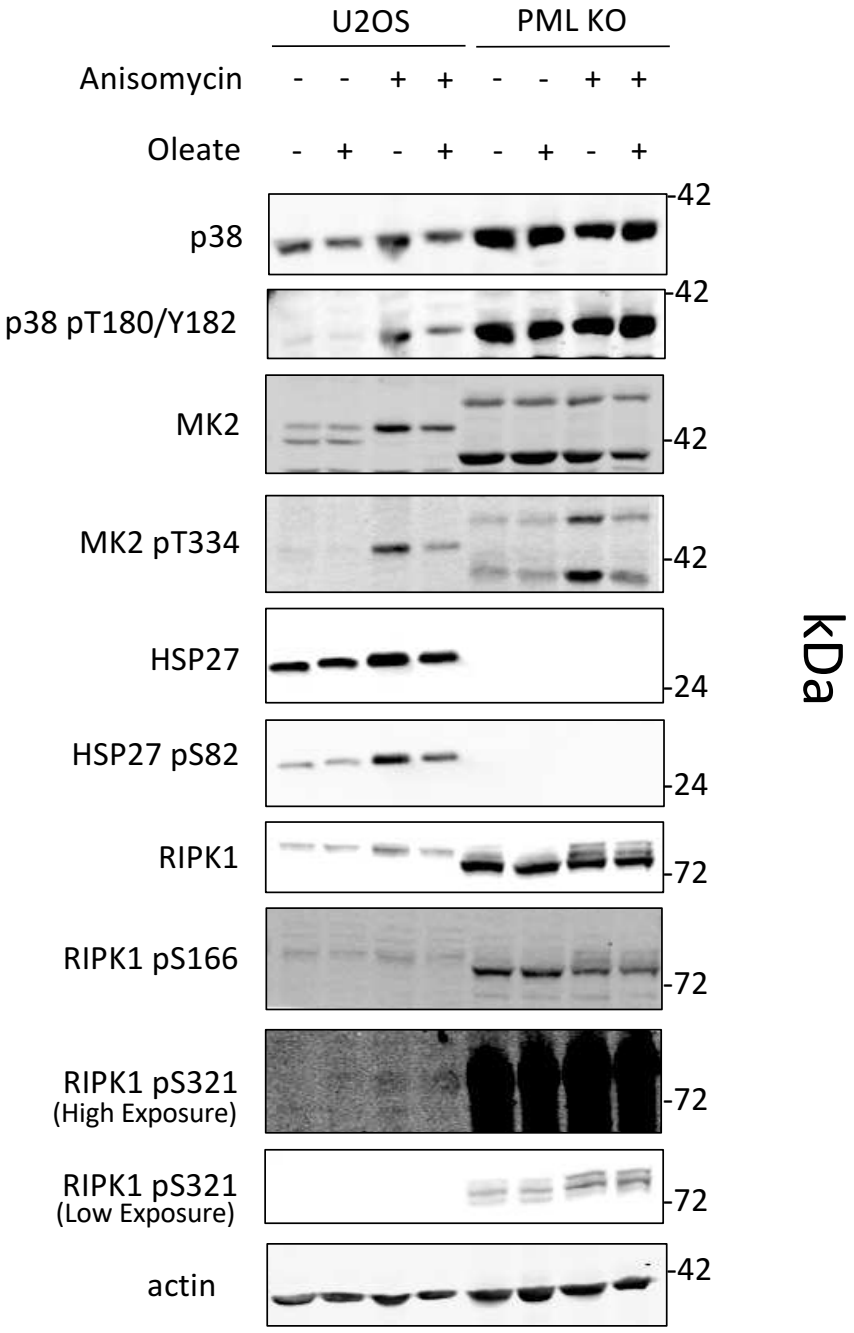

Figure 3.18 Severe dysregulation of p38 phosphorylation cascade in PML KO cells. U2OS cells were treated with 500 μM oleate for 24 h before being treated acutely with 0.5 μM anisomycin for 30 mins. Lysates cells were then prepared and resolved by SDS-PAGE and transferred to nitrocellulose. Immunoblotted with anti-p38 (1:1000), anti-p38 pT180/Y182 (1:1000), anti-MK2 (1:500), anti-MK2 pT334 (1:1000), anti-HSP27 (1;1000), anti-HSP27 pS82 (1:1000), anti-RIPK1 (1:1000), anti-RIPK1 pS166 (1:1000), anti-RIPK1 pS321 (1:1000), or anti-actin (1:20000).

with and without oleate that were not treated with anisomycin. This indicates that under basal conditions, LAPS formation have no effect on the p38 pathway. In U2OS cells treated with anisomycin regardless of oleate treatment, there was an increase in phosphorylation for p38 pT180/Y182, MK2 pT334, HSP27 pS82, RIPK1 pS166, and RIPK1 pS321. This indicates that anisomycin was stimulating the p38 kinase cascade as expected. With respect to differences in phosphorylation relative to protein expression between oleate treatment in cells also treated with anisomycin, there was no change in p38 pT180/Y182, but there was a slight reduction in MK2 pT334. Under these conditions, the standardize phosphorylation levels were reduced by 40% in the oleate treated cells in comparison to the untreated cells. This signal reduction was not maintained by the standardized HSP27 pS82 signal which was only reduced by 10%. This indicated that under stress conditions caused by anisomycin, oleate treatment affects MK2 phosphorylation, but that this reduction is not maintained for downstream phosphorylation targets. Further the lack in increase in RIPK1 pS166 in oleate treated U2OS cells indicates that LAPS formation does not play a role in RIPK1 mediated necroptosis.

In U2OS PML KO cells there was increased p38 protein expression and p38 pT180/Y182 signal relative to U2OS cells regardless of anisomycin or oleate treatment. The protein MK2 now had two different protein masses, one at approximately 47 kDa and the other at approximately 39 kDa. There was also increased protein expression of these new molecular mass proteins relative to the U2OS cells. Additionally, these proteins also had basal MK2 pT334 signal when not treated with anisomycin that increased with treatment. While the lower band could be the result of alternate splicing,

and correspond to a predicted isoforms determined computationally, the upper band does not and could be due to post-translational modification. There was no expression of HSP27 in the U2OS PML KO cells suggesting that HSP27 protein expression is PML dependent. Lastly, there was increased expression of RIPK1 relative to U2OS cells that was accompanied by increased RIPK1 pS166 and pS321 signal. This would indicate that there was increased RIPK1 pS166 mediated necroptosis, even with the increased inhibitory RIPK1 pS321 signal that prevents RIPK1 pS166 autophosphorylation. Taken together, these data demonstrate that there is severe dysregulation of expression and phosphorylation of proteins in the p38 cascade in the absence of PML.

Chapter 4: Discussion

4.1 Analysis of PML Interactome

The PML interactome generated from APEX2 proximity labelling found a multitude of high confidence interactors. Using the data base BioGRID, I was able to compare which of my high confidence interactors have been found to associate with other known interactors of PML (**Figure 4.1**) [97]. Of my 66 high confidence interactors, LPP, PPP1R13L, STAM, SEC24B, TNKS1BP1, IGBP1, and ERCC6L were also found to be high confidence interactors of TurboID-PML from Barroso-Gomila et al. (2021) while the protein CSNK1D was found from affinity capture-western methods performed by Alsheich-Bartok et al. (2008) [79, 98]. The protein MK2 was not a part of this database but had been previously established to interact with PML (**Figure 3.7 & 3.8**). While the small portion of previously known high confidence interactors may be cause for concern, there are a few important details to outline with respect to thresholding, PML diversity and novel identification of protein interactions.

Firstly, from the raw data set I did find other known PML protein interactors; DAXX, SP100, Lipin-1, SUMO-1, and other SUMO interacting proteins were identified but did not make either the SAINT score cut offs or pass the Bayesian false discovery rate threshold. These proteins would have obviously passed the CRAPome filter as they are not common contaminants of proteomic analysis. This indicates that there was not enough of enrichment of APEX2-mediated biotinylation of these known PML interactors to draw significance from the two different analyses. This is indicative of a high false negative rate. However, given that the objective of thresholding was to be as stringent as

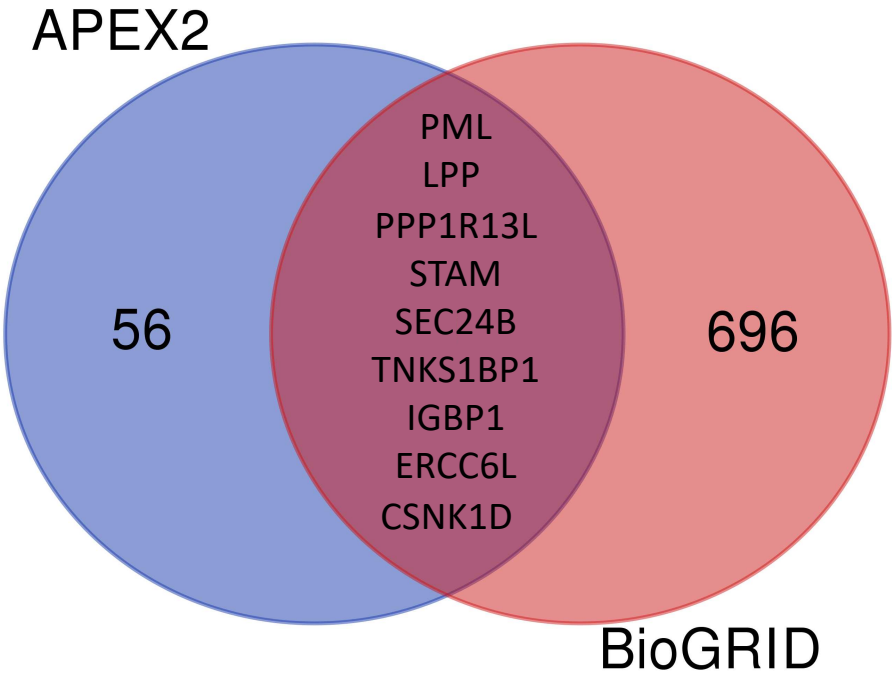

Figure 4.1. Overlap of Identified Proteins Between the APEX2-PML Interactome and BioGRID. The list of high confidence interactors were queried against all the known interactors of PML from BioGRID. There were 9 overlapping proteins. Of these proteins LPP, PP1R13L, STAM, SEC24B, TNKS1BP1, IGBP1, and ERCC6L were identified by Barroso-Gomila et al. (2021), and CSNK1D was identified by Alsheich-Bartok et al. (2008).

possible, the test would naturally skew towards a high a false negative rate to maintain a high true positive rate.

One of the reasons that there was not enough enrichment might be due to the high structural diversity of PML. Given PML is a scaffold protein, it coordinates the recruitment of other proteins that allow the larger PML structure to perform specific cellular functions [46]. There are many different types of nuclear PML structures pertinent to the conditions the proximity labelling. PML could be forming alternative lengthening of telomeres (ALT) associated PML bodies (APB) [99], mitotic accumulation of PML proteins (MAPP) [100], or nucleolar caps [101] in addition to PML-NBs and LAPS. These PML structures have different proteomes and could be labelled under the conditions of the experiment. Further, the physical structure heterogeneity of PML-NBs and LAPS could be affecting the APEX2 protein ability to biotinylate nearby proteins. PML-NBs are spherical structures that form when PML becomes SUMOylated. The proteins that attach to the PML-NB through SUMO or SIM interactions occur at the center core of the nuclear body [102]. The location of PML on the outside of the nuclear body with the associated proteins at the center core could decrease the efficiency of labelling these associated proteins. LAPS are also not homogenous structures. Super-resolution radial fluctuation (SRRF) imaging of LAPS has demonstrated that different proteins associate at different polar locations on the nLD. PML associates at the top of the nLD as a cap, that slightly overlaps with the protein CCTα associating near the bottom [19]. This separation of proteins on nLDs may indicate why in the unfiltered data set there was no identification of the CCTα.

The APEX2-PML interactome dot plot shows that interacting proteins skewed in two different directions (**Figure 3.7**). Firstly, comparing oleate treated and untreated conditions, there were many more proteins found under the oleate treated conditions. This can be attributed to the increased surface area on LAPS that APEX-HA-PML bind to allowing for concentrated biotinylation of other prey proteins. Secondly, with respect to the PML isoform distribution, there was more confidence and quantity found with PML-I. This may be due to APEX2-HA-PML-I expression in U2OS cells which express endogenous PML-I and PML-II [103]. If the interactions were PML-I specific, proximity labelling in U2OS cells could cause the APEX2-HA-PMLII interacting with LAPS to label endogenous PML-I interactions. In hindsight, this could be remedied by preforming the proximity labeling in the U2OS PML KO cells, however the severe dysregulation of the p38 cascade and absence of HSP27 expression is indicative of an altered signalling cascade in this cell line (**Figure 3.18**). If the wildtype phenotype was restored from transient transfection of the APEX2-PML constructs, this could be an improvement on the experimental design. However, there would be issues of PML-II dependant nLD formation not occurring and other PML interactions that require multiple isoforms present.

Of the network of proteins that were identified in the PML-APEX interactome, there was one large cluster of ESCRT and COP-II proteins (**Figure 3.8**). Both these pathways are involved in vesicular formation however they are used for trafficking cellular cargo for different purposes. The proteins STAM and SEC24B were identified by Barroso-Gomila et al. (2021) and are components of the ESCRT and COP-II complexes

respectively. In the following paragraphs I will outline the connections between these two cellular mechanisms and LDs.

ESCRT complexes are involved in the recruitment of ubiquitinated proteins into the endosome allowing for multivesicular bodies (MVB) biogenesis [104]. These MVBs are then degraded following their fusion with lysosomes [105]. There are multiple ESCRT complexes that work in conjunction to form MVB. ESCRT complex-1 protein TSG101 and ESCRT complex-0 proteins STAM, and STAM2 were identified from the list of high confidence PML-APEX interactors. A recent paper demonstrated that through the cooperation of ESCRT protein VPS13D**,** TSG101 facilitated the transfer of FAs from cLDs to mitochondria during cell starvation by deforming the cLD phospholipid monolayer to allow access to the TAG core [106]. While this is a cLD interaction, TSG101 is found in the nucleus of cells [107].

The COP-II group of proteins are involved in vesicle formation for the anterograde transportation of proteins from the ER to the Golgi apparatus [108]. From the list of high confidence APEX-PML interactors, SEC23B, SEC24A, SEC24B, and SEC23IP were identified, all of which are components of the COP-II complex. The protein Sec23B interacts with cLDs as well and facilitates delivering ATGL to the LD. It was determined that this interaction was occurring at ER exit-sites and ER-Golgi intermediate compartment [38, 109]. These sites are utilized by the cells to accumulate cargo that will be transported in a COP-II-dependant manner. While the LD interaction was occurring in the cytoplasm, SEC23B has been identified to interact with ER stress proteins in the nucleus of cells [110]. This gives the PML interaction plausibility given

the nuclear localization along with a function that is hypothesized to be shared with nLDs.

4.2 PML-I Associates with MK2

The data demonstrating that PML colocalizes with MK2 on both PML-NBs and nLDs (**Figure 3.9-3.12**), expands and validates the research performed by Chen et al. (2021). They demonstrated using IF and co-immunoprecipitation techniques that the proline-rich region at the N-terminus of MK2-II facilitates the its interaction with PML-I in HEK293T cells [95]. The expression of GFP-PML into U2OS PML KO cells of shows that the interaction between MK2 and PML is occurring not only with respect with the N terminal region of MK2, but also the exon 9 region of PML (**Figure 3.13**). Exon-9 in the PML gene contains a nuclear export signal and an exonuclease-III-like motif [111]. Studies have shown that unique protein-protein interactions occur at the C-terminus of the PML, which these structural features may be facilitating [112]. While my data demonstrates that the C-terminus of PML is forming this interaction, MK2 is also SUMOylated at lysine 339 [112]. However, current evidence argues against PML-MK2 interaction occurring through SUMO-SIM binding, as the MK2 N-terminal region and PML C-terminal region facilitates the interaction. This is opposite to C-terminal SUMO sites of MK2 and the SIM site located in the middle of PML [113]. While our data also suggests that the interaction is occurring through PML-I, their data does not address MK2 interactions with other PML isoforms [95]. Together, our data suggests that this interaction is not cell line specific, but occurs in U2OS, Huh7 and HEK293T cells.

The raw data LC-MS/MS data on the MK2 interaction identified 4 unique MK2 peptide fragments. Three of the peptides are shared sequence between the isoforms 1 and II of MK2, while one was unique to the C-terminus of MK2-II that contains the NLS. While I was able to show through IF confocal imaging that both isoforms interact with LAPS, the LC-MS/MS data cannot differentiate the shorter MK2-I from the longer MK2-II.

Looking at the spatial distribution of MK2-II association with nLDs, there is a unique pattern of MK2 coating the top of the nLD, outside of the PML shell (**Figure 3.11**). The evidence of MK2 associating with nLDs in a PML dependant manner, is consistent with the evidence that PML coats the tops of LAPS [19]. While the MK2-II signal is seen throughout the nucleus, only when the protein is associating with LAPS is when there was a change in its spatial distribution. This is most likely a function of overexpression, which could be improved by tagging the endogenous protein using a CRISPR knock in system.

The smaller MK2-I isoform that does not contain the NLS was observed to be interacting with PML inside the nucleus. Given this isoform of MK2 is 42 kDa, it could pass through the nuclear pore complex by passive diffusion since it excludes proteins of 60 kDa or larger [114]. This data is also confirmed by the co-immunoprecipitation experiment performed by Chen et al. (2021), where they demonstrated that PML-1 was associating with this isoform, even though it does not contain a NLS [95].

4.3 Dysregulation of p38 cascade in U2OS PML KO Cells

The extreme dysregulation of the p38 cascade seen in the U2OS PML KO cells (**Figure 3.18**) was also partially observed in the paper by Chen et al, (2021). Though they treated MEF cells with both zVAD and AT-406 to induce cell death by necroptosis, both their and my data showed that there was increased phosphorylation of p38 T180/Y182, MK2 T334, and RIPK1 S321 in PML KO cells [95]. Given the hyper-phosphorylation of p38 in the PML KO cells, this is to be expected as the kinase cascade would cause phosphorylation of each downstream protein. However, there was disagreement with my data that demonstrated RIPK1 S166 was also hyper phosphorylated in the PML KO cells. It is established in literature that active MK2 phosphorylates RIPK1 at S321 causing suppression of autophosphorylation of the RIPK1 S166 [92]. RIPK1 S166 phosphorylation is responsible for the induction of mixed lineage kinase domain-like (MLKL) activity that ruptures organelle membranes resulting in necroptosis [115]. The increase in RIPK1 pS166 regardless of p38 stimulation by anisomycin treatment or LAPS formation by oleate treatment indicates that this is a phenotype of the U2OS PML KO cells. This could be due to differences between MEF and U2OS cells, or due to an off-target effect of the CRISPR/Cas9 gene editing. Replication of this experiment in other cell lines might provide a definitive answer. Alternately, treating the U2OS PML KO cells with zVAD and AT-406 could show whether this cell line is more prone to necroptosis.

The slight reduction in MK2 pT334 in the U2OS cells treated with both anisomycin and oleate relative to cells treated with anisomycin alone may be indicative of LAPS formation altering MK2 phosphorylation. However, this slight reduction was

not apparent for downstream HSP27 phosphorylation, which maintains a similar phosphorylation signal when the kinase cascade was stimulated with anisomycin regardless of oleate treatment. Given the nature of signal amplification from kinase cascades, the slight reduction in MK2 phosphorylation may not be sufficient to have downstream effects. Further experimental replicates are needed to confirm this result.

4.4 PML is Required for HSP27 Expression

One of the most striking results from studying the p38 cascade in U2OS and U2OS PML KO cells was the inhibition of HSP27 expression (**Figure 3.18**). There are no reports that PML is required for HSP27 protein expression, however these two proteins are linked through their interactions with DAXX in multiple cellular signalling pathways (**Figure 4.2**). Firstly, DAXX interacts with the TNFα receptor, which in turn stimulates the p38 phosphorylation cascade resulting in MK2 phosphorylation of HSP27 [91, 116]. Phosphorylated HSP27 is also involved in the inhibition of DAXX associating with the FAS receptor, blocking FAS mediated apoptosis [117]. Phosphorylated HSP27 also inhibits DAXX export from the nucleus to the cytoplasm when it is no longer associated with PML [117]. With the multiple interactions between DAXX, HSP27 and PML could explain this result. However, the lack of protein expression could also be attributed to the dysregulation of the p38 cascade in the U2OS PML KO cells. Screening other PML KO cells for HSP27 expression, along with re-expressing PML in the PML KO cells to determine if HSP27 expression can be rescued would validate this observation.

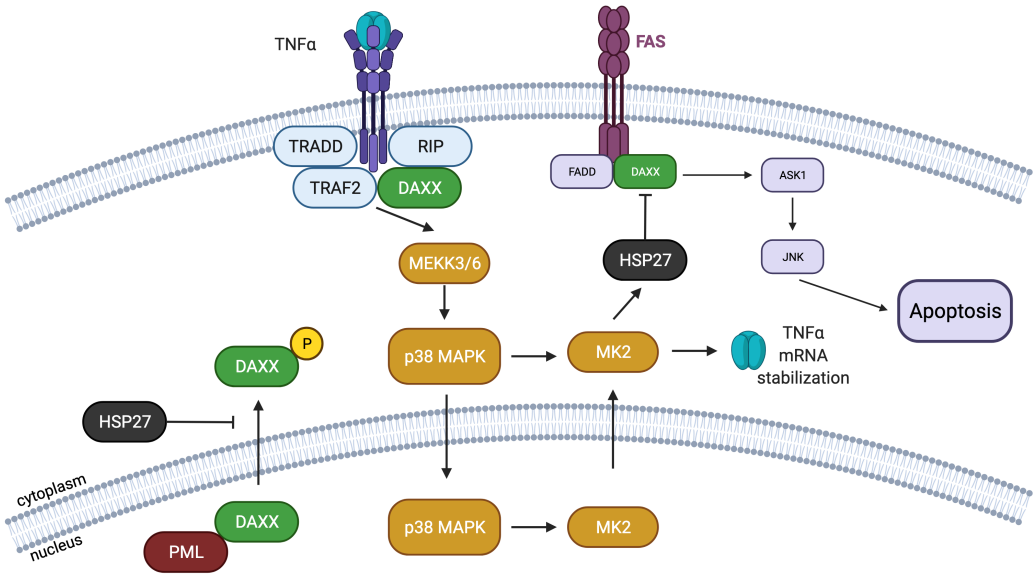

Figure 4.2. Interactions between DAXX, MK2 and HSP27. TNFα mediated activation of the p38 cascade requires DAXX interaction with TNFα receptor. The p38 phosphorylation cascade Results in MK2 phosphorylation of HSP27. Phosphorylated HSP27 inhibits DAXX from associating with the FAS receptor, blocking FAS mediated apoptosis. Phosphorylated HSP27 inhibits DAXX export from the nucleus to the cytoplasm when it is no longer associated with PML.

4.5 MK2 Inhibits LAPS Formation

The inhibition of MK2 phosphorylation caused an increase in LAPS formation, while inhibition of p38 phosphorylation was not statistically different from the control. This result is peculiar given that p38 phosphorylation activates MK2 (**Figure 3.15).** One would expect that treatments with p38 and MK2 inhibitors would have the same effect on LAPS formation. However, p38 phosphorylation is required for interferon stimulated response elements (ISRE) and interferon-γ activated sequences (GAS) gene expression [118]. The PML gene promoter contains both regulatory elements, and p38 phosphorylation has been shown to activate PML gene expression [119]. Given PML is required for LAPS formation, the inhibition of p38 would therefore decrease LAPS formation through this mechanism. With respect to MK2 phosphorylation inhibition, there was a statistically significant increase in LAPS formation. This would be indicative of an unknown protein that negatively regulates LAPS formation when phosphorylated by MK2. p38 could regulate LAPs formation positively through IRSE and GAS elements, and negatively through MK2 (**Figure 4.3**). The lack of statistical difference might indicate these two regulatory mechanisms cancelling each other out. It is also possible that this an off-target effect from the drug treatment biasing the quantification.

Experimentally, the siRNA knock-down of MK2 could show that LAPS formation was caused by MK2 phosphorylation or an off-target effect from the inhibitor. Western blots shows that the MK2 siRNA produced an approximately 80 % knockdown (**Figure 3.16**). However, the results demonstrate that there was no statistical difference in LAPS/cell with the siRNA knock down (**Figure 3.17**). Since this was not a complete knockdown of MK2 and kinase cascades by their nature amplify cellular signals, the

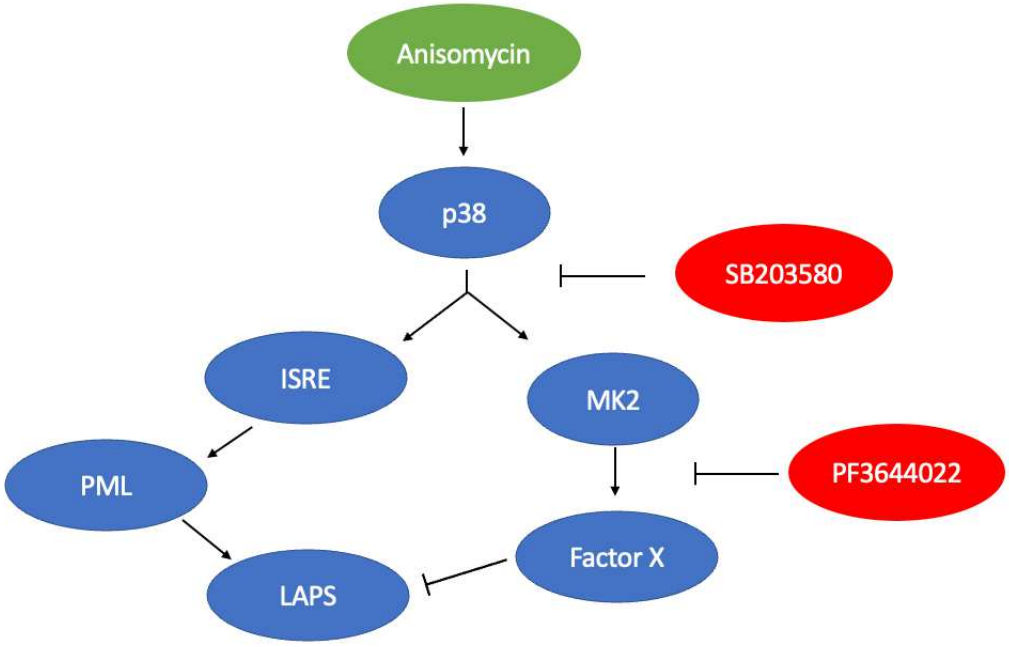

Figure 4.3. Proposed model of how MK2 inhibits LAPS formation. The p38 kinase inhibitor SB-203580 blocks both PML gene transcription interferon stimulated response element resulting in less LAPS formation. This also blocks MK2 phosphorylation. Inhibition of MK2 phosphorylation with PF-3644022 causes an increase in LAPS formation though phospho-regulation of unknown Factor X that inhibits LAPS formation when phosphorylated. PML upregulation increasing LAPS formation and Factor X decreasing LAPS formation are aneled out with SB-203480 treatment.

residual MK2 might be sufficient to maintain the same phenotype. Observing HSP27 phosphorylation in anisomycin treated cells that have MK2 knocked down would address this hypothesis. Alternatively, using CRISPR to completely knock out MK2 would also determine if MK2 inhibits LAPS formation.

4.6 Conclusions

This investigation utilized proximity labelling with APEX2 conjugated PML constructs to biotinylate nearby protein interactors on PML nuclear bodies and LAPS in U2OS cells. This allowed for the creation of a PML isoform specific interactome under these conditions. From this list of high confidence interactors, the protein MK2 was identified as a candidate for further investigation given previous research on its interaction with PML. This was the first study to show using IF imaging that MK2 associates with LAPS. Additionally, I demonstrated that MK2 phosphorylation may be regulating LAPS formation, but more verification of the mechanism is required. Lastly, I demonstrated that oleate treatment did not affect the p38 phosphorylation cascade, but that the lack of PML severely dysregulated the phosphorylation and expression of multiple proteins in the pathway. Additional studies are required to validate other candidate interactors of PML identified through proximity labelling and determine how LAPS and MK2 phosphorylation are connected.

References

1. Fujimoto, T. and R.G. Parton, *Not just fat: the structure and function of the lipid droplet.* Cold Spring Harbor perspectives in biology, 2011. **3**(3): p. a004838.

2. Horn, P.J., et al., *Visualization of lipid droplet composition by direct organelle mass spectrometry.* Journal of Biological Chemistry, 2011. **286**(5): p. 3298-3306.

3. Rambold, A.S., S. Cohen, and J. Lippincott-Schwartz, *Fatty acid trafficking in starved cells: regulation by lipid droplet lipolysis, autophagy, and mitochondrial fusion dynamics.* Developmental cell, 2015. **32**(6): p. 678-692.

4. Hashimoto, T., et al., *Active involvement of micro-lipid droplets and lipid-droplet-associated proteins in hormone-stimulated lipolysis in adipocytes.* Journal of cell science, 2012. **125**(24): p. 6127-6136.

5. Wang, C.-W., *Lipid droplets, lipophagy, and beyond.* Biochimica et Biophysica Acta (BBA)-Molecular and Cell Biology of Lipids, 2016. **1861**(8): p. 793-805.

6. Dong, H. and M.J. Czaja, *Regulation of lipid droplets by autophagy.* Trends in Endocrinology & Metabolism, 2011. **22**(6): p. 234-240.

7. Barbosa, A.D., D.B. Savage, and S. Siniossoglou, *Lipid droplet–organelle interactions: emerging roles in lipid metabolism.* Current opinion in cell biology, 2015. **35**: p. 91-97.

8. Sturley, S.L. and M.M. Hussain, *Lipid droplet formation on opposing sides of the endoplasmic reticulum.* Journal of lipid research, 2012. **53**(9): p. 1800-1810.

9. Benador, I.Y., et al., *Mitochondria bound to lipid droplets: where mitochondrial dynamics regulate lipid storage and utilization.* Cell metabolism, 2019. **29**(4): p. 827-835.

10. Binns, D., et al., *An intimate collaboration between peroxisomes and lipid bodies.* The Journal of cell biology, 2006. **173**(5): p. 719-731.

11. Olzmann, J.A. and P. Carvalho, *Dynamics and functions of lipid droplets.* Nature reviews Molecular cell biology, 2019. **20**(3): p. 137-155.

12. Ogasawara, Y., et al., *Long-term autophagy is sustained by activation of CCTβ3 on lipid droplets.* Nature communications, 2020. **11**(1): p. 1-12.

13. Layerenza, J.P., et al., *Nuclear lipid droplets: a novel nuclear domain.* Biochimica et Biophysica Acta (BBA)-Molecular and Cell Biology of Lipids, 2013. **1831**(2): p. 327-340.

14. Uzbekov, R. and P. Roingeard, *Nuclear lipid droplets identified by electron microscopy of serial sections.* BMC Research Notes, 2013. **6**(1): p. 1-4.

15. Yue, L., et al., *Differential dephosphorylation of CTP: phosphocholine cytidylyltransferase upon translocation to nuclear membranes and lipid droplets.* Molecular biology of the cell, 2020. **31**(10): p. 1047-1059.

16. Sołtysik, K., et al., *Nuclear lipid droplets derive from a lipoprotein precursor and regulate phosphatidylcholine synthesis.* Nature communications, 2019. **10**(1): p. 1-12.

17. Ohsaki, Y., et al., *PML isoform II plays a critical role in nuclear lipid droplet formation.* Journal of Cell Biology, 2016. **212**(1): p. 29-38.

18. Mosquera, J.V., M.C. Bacher, and J.R. Priess, *Nuclear lipid droplets and nuclear damage in Caenorhabditis elegans.* PLoS Genetics, 2021. **17**(6): p. e1009602.

19. Lee, J., et al., *Lipid-associated PML domains regulate CCTα, Lipin1 and lipid homeostasis.* bioRxiv, 2020.

20. Walther, T.C., J. Chung, and R.V. Farese Jr, *Lipid droplet biogenesis.* Annual review of cell and developmental biology, 2017. **33**: p. 491.

21. Chung, J., et al., *LDAF1 and seipin form a lipid droplet assembly complex.* Developmental cell, 2019. **51**(5): p. 551-563. e7.

22. Wilfling, F., et al., *Triacylglycerol synthesis enzymes mediate lipid droplet growth by relocalizing from the ER to lipid droplets.* Developmental cell, 2013. **24**(4): p. 384-399.

23. Stone, S.J., M.C. Levin, and R.V. Farese, *Membrane topology and identification of key functional amino acid residues of murine acyl-CoA: diacylglycerol acyltransferase-2.* Journal of Biological Chemistry, 2006. **281**(52): p. 40273-40282.

24. Blanchette-Mackie, E.J., et al., *Perilipin is located on the surface layer of intracellular lipid droplets in adipocytes.* Journal of lipid research, 1995. **36**(6): p. 1211-1226.

25. Romanauska, A. and A. Köhler, *The inner nuclear membrane is a metabolically active territory that generates nuclear lipid droplets.* Cell, 2018. **174**(3): p. 700-715. e18.

26. Kornke, J.M. and M. Maniak, *Fat-containing cells are eliminated during Dictyostelium development.* Biology open, 2017. **6**(9): p. 1294-1304.

27. Mcphee, M.J., et al., *Running'LAPS'around nLD: Nuclear lipid droplet form and function.* Frontiers in Cell and Developmental Biology, 2022: p. 88.

28. Infante, J.P., *Rate-limiting steps in the cytidine pathway for the synthesis of phosphatidylcholine and phosphatidylethanolamine.* Biochemical Journal, 1977. **167**(3): p. 847.

29. Fraga, M.F. and M. Esteller, *Epigenetics and aging: the targets and the marks.* TRENDS in Genetics, 2007. **23**(8): p. 413-418.

30. Shumaker, D.K., et al., *Mutant nuclear lamin A leads to progressive alterations of epigenetic control in premature aging.* Proceedings of the National Academy of Sciences, 2006. **103**(23): p. 8703-8708.

31. Drané, P., et al., *The death-associated protein DAXX is a novel histone chaperone involved in the replication-independent deposition of H3. 3.* Genes & development, 2010. **24**(12): p. 1253-1265.

32. Finck, B.N. and D.P. Kelly, *PGC-1 coactivators: inducible regulators of energy metabolism in health and disease.* The Journal of clinical investigation, 2006. **116**(3): p. 615-622.

33. Rosen, E.D., et al., *C/EBPα induces adipogenesis through PPARγ: a unified pathway.* Genes & development, 2002. **16**(1): p. 22-26.

34. Lamming, D.W. and D.M. Sabatini, *A central role for mTOR in lipid homeostasis.* Cell metabolism, 2013. **18**(4): p. 465-469.

35. Bosch, M., et al., *Mammalian lipid droplets are innate immune hubs integrating cell metabolism and host defense.* Science, 2020. **370**(6514): p. eaay8085.

36. Krahmer, N., et al., *Phosphatidylcholine synthesis for lipid droplet expansion is mediated by localized activation of CTP: phosphocholine cytidylyltransferase.* Cell metabolism, 2011. **14**(4): p. 504-515.

37. Kuerschner, L., C. Moessinger, and C. Thiele, *Imaging of lipid biosynthesis: how a neutral lipid enters lipid droplets.* Traffic, 2008. **9**(3): p. 338-352.

38. Soni, K.G., et al., *Coatomer-dependent protein delivery to lipid droplets.* Journal of cell science, 2009. **122**(11): p. 1834-1841.

39. Brasaemle, D.L., *The perilipin family of structural lipid droplet proteins: stabilization of lipid droplets and control of lipolysis.* J Lipid Res, 2007. **48**(12): p. 2547-2559.

40. McMaster, C.R. and R.M. Bell, *CDP-choline: 1, 2-diacylglycerol cholinephosphotransferase.* Biochimica et Biophysica Acta (BBA)-Lipids and Lipid Metabolism, 1997. **1348**(1-2): p. 100-110.

41. Arnold, R.S. and R.B. Cornell, *Lipid regulation of CTP: phosphocholine cytidylyltransferase: electrostatic, hydrophobic, and synergistic interactions of anionic phospholipids and diacylglycerol.* Biochemistry, 1996. **35**(30): p. 9917-9924.

42. Duden, R., *ER-to-Golgi transport: Cop I and Cop II function.* Molecular membrane biology, 2003. **20**(3): p. 197-207.

43. Jensen, K., C. Shiels, and P.S. Freemont, *PML protein isoforms and the RBCC/TRIM motif.* Oncogene, 2001. **20**(49): p. 7223-7233.

44. Nisole, S., et al., *Differential roles of PML isoforms.* Frontiers in oncology, 2013. **3**: p. 125.

45. Van Damme, E., et al., *A manually curated network of the PML nuclear body interactome reveals an important role for PML-NBs in SUMOylation dynamics.* Int J Biol Sci, 2010. **6**(1): p. 51-67.

46. Lallemand-Breitenbach, V. and H. de Thé, *PML nuclear bodies: from architecture to function.* Current opinion in cell biology, 2018. **52**: p. 154-161.

47. Duprez, E., et al., *SUMO-1 modification of the acute promyelocytic leukaemia protein PML: implications for nuclear localisation.* Journal of Cell Science, 1999. **112**(3): p. 381-393.

48. Hoischen, C., et al., *Multimodal Light Microscopy Approaches to Reveal Structural and Functional Properties of Promyelocytic Leukemia Nuclear Bodies.* Front Oncol, 2018. **8**: p. 125.

49. Stehmeier, P. and S. Muller, *Phospho-regulated SUMO interaction modules connect the SUMO system to CK2 signaling.* Mol Cell, 2009. **33**(3): p. 400-9.

50. Hecker, C.-M., et al., *Specification of SUMO1-and SUMO2-interacting motifs.* Journal of Biological Chemistry, 2006. **281**(23): p. 16117-16127.

51. Ohbayashi, N., et al., *The IL-6 family of cytokines modulates STAT3 activation by desumoylation of PML through SENP1 induction.* Biochem Biophys Res Commun, 2008. **371**(4): p. 823-8.

52. Padmakumar, V., et al., *The inner nuclear membrane protein Sun1 mediates the anchorage of Nesprin-2 to the nuclear envelope.* Journal of cell science, 2005. **118**(15): p. 3419-3430.

53. Kumar, D., et al., *REEP3 and REEP4 determine the tubular morphology of the endoplasmic reticulum during mitosis.* Molecular biology of the cell, 2019. **30**(12): p. 1377-1389.

54. Goulbourne, C.N., A.N. Malhas, and D.J. Vaux, *The induction of a nucleoplasmic reticulum by prelamin A accumulation requires CTP: phosphocholine cytidylyltransferase-α.* Journal of cell science, 2011. **124**(24): p. 4253-4266.

55. Wang, M., et al., *PML2-mediated thread-like nuclear bodies mark late senescence in Hutchinson–Gilford progeria syndrome.* Aging Cell, 2020. **19**(6): p. e13147.

56. Grasso, C.S., et al., *The mutational landscape of lethal castration-resistant prostate cancer.* Nature, 2012. **487**(7406): p. 239-243.

57. Chen, M., et al., *An aberrant SREBP-dependent lipogenic program promotes metastatic prostate cancer.* Nature genetics, 2018. **50**(2): p. 206-218.

58. Carracedo, A., et al., *A metabolic prosurvival role for PML in breast cancer.* The Journal of clinical investigation, 2012. **122**(9): p. 3088-3100.

59. Popescu, C.I. and J. Dubuisson, *Role of lipid metabolism in hepatitis C virus assembly and entry.* Biology of the Cell, 2010. **102**(1): p. 63-74.

60. Syed, G.H., Y. Amako, and A. Siddiqui, *Hepatitis C virus hijacks host lipid metabolism.* Trends in Endocrinology & Metabolism, 2010. **21**(1): p. 33-40.

61. Scorletti, E. and R.M. Carr, *A new perspective on NAFLD: Focusing on lipid droplets.* Journal of Hepatology, 2021.

62. Hashimoto, E., M. Taniai, and K. Tokushige, *Characteristics and diagnosis of NAFLD/NASH.* Journal of gastroenterology and hepatology, 2013. **28**: p. 64-70.

63. M'barek, K.B., et al., *ER membrane phospholipids and surface tension control cellular lipid droplet formation.* Developmental cell, 2017. **41**(6): p. 591-604. e7.

64. BasuRay, S., et al., *Accumulation of PNPLA3 on lipid droplets is the basis of associated hepatic steatosis.* Proceedings of the National Academy of Sciences, 2019. **116**(19): p. 9521-9526.

65. Fujii, H., et al., *Expression of perilipin and adipophilin in nonalcoholic fatty liver disease; relevance to oxidative injury and hepatocyte ballooning.* Journal of atherosclerosis and thrombosis, 2009: p. 0912210123-0912210123.

66. McManaman, J.L., et al., *Perilipin-2-null mice are protected against diet-induced obesity, adipose inflammation, and fatty liver disease [S].* Journal of lipid research, 2013. **54**(5): p. 1346-1359.

67. Carr, R.M. and R.S. Ahima, *Pathophysiology of lipid droplet proteins in liver diseases.* Experimental cell research, 2016. **340**(2): p. 187-192.

68. Magné, J., et al., *The minor allele of the missense polymorphism Ser251Pro in perilipin 2 (PLIN2) disrupts an α-helix, affects lipolysis, and is associated with reduced plasma triglyceride concentration in humans.* The FASEB Journal, 2013. **27**(8): p. 3090-3099.

69. Sanyal, A.J., et al., *Nonalcoholic steatohepatitis: association of insulin resistance and mitochondrial abnormalities.* Gastroenterology, 2001. **120**(5): p. 1183-1192.

70. Zhang, X. and K. Zhang, *Endoplasmic reticulum stress-associated lipid droplet formation and type II diabetes.* Biochemistry research international, 2012. **2012**.

71. Dyal, H.K., et al., *Concurrent obesity, diabetes, and steatosis increase risk of advanced fibrosis among HCV patients: a systematic review.* Digestive diseases and sciences, 2015. **60**(9): p. 2813-2824.

72. Reaven, G., F. Abbasi, and T. McLaughlin, *Obesity, insulin resistance, and cardiovascular disease.* Recent progress in hormone research, 2004. **59**: p. 207-224.

73. Shulman, G.I., *Cellular mechanisms of insulin resistance.* The Journal of clinical investigation, 2000. **106**(2): p. 171-176.

74. Gaggini, M., et al., *Non-alcoholic fatty liver disease (NAFLD) and its connection with insulin resistance, dyslipidemia, atherosclerosis and coronary heart disease.* Nutrients, 2013. **5**(5): p. 1544-1560.

75. Lam, S.S., et al., *Directed evolution of APEX2 for electron microscopy and proximity labeling.* Nature methods, 2015. **12**(1): p. 51-54.

76. Hwang, J. and P.J. Espenshade, *Proximity-dependent biotin labelling in yeast using the engineered ascorbate peroxidase APEX2.* Biochemical Journal, 2016. **473**(16): p. 2463-2469.

77. Roux, K.J., et al., *A promiscuous biotin ligase fusion protein identifies proximal and interacting proteins in mammalian cells.* Journal of Cell Biology, 2012. **196**(6): p. 801-810.

78. Kim, D.I., et al., *Probing nuclear pore complex architecture with proximity-dependent biotinylation.* Proceedings of the National Academy of Sciences, 2014. **111**(24): p. E2453-E2461.

79. Barroso-Gomila, O., et al., *Identification of proximal SUMO-dependent interactors using SUMO-ID.* Nature communications, 2021. **12**(1): p. 1-19.

80. May, D.G., et al., *Comparative application of BioID and TurboID for protein-proximity biotinylation.* Cells, 2020. **9**(5): p. 1070.

81. Pinder, J., J. Salsman, and G. Dellaire, *Nuclear domain 'knock-in' screen for the evaluation and identification of small molecule enhancers of CRISPR-based genome editing.* Nucleic Acids Research, 2015. **43**(19): p. 9379-9392.

82. Attwood, K.M., et al., *PML isoform expression and DNA break location relative to PML nuclear bodies impacts the efficiency of homologous recombination.* Biochemistry and Cell Biology, 2019. **98**(3): p. 314-326.

83. Sultana, S., J. Stewart, and A.C. van der Spoel, *Truncated mutants of beta-glucosidase 2 (GBA2) are localized in the mitochondrial matrix and cause mitochondrial fragmentation.* Plos one, 2020. **15**(6): p. e0233856.

84. Del Olmo, T., et al., *APEX2-mediated RAB proximity labeling identifies a role for RAB21 in clathrin-independent cargo sorting.* EMBO reports, 2019. **20**(2): p. e47192.

85. Cox, J. and M. Mann, *MaxQuant enables high peptide identification rates, individualized p.p.b.-range mass accuracies and proteome-wide protein quantification.* Nature Biotechnology, 2008. **26**(12): p. 1367-1372.

86. Mellacheruvu, D., et al., *The CRAPome: a contaminant repository for affinity purification–mass spectrometry data.* Nature Methods, 2013. **10**(8): p. 730-736.

87. Teo, G., et al., *SAINTexpress: improvements and additional features in Significance Analysis of INTeractome software.* J Proteomics, 2014. **100**: p. 37-43.

88. Knight, J.D.R., et al., *ProHits-viz: a suite of web tools for visualizing interaction proteomics data.* Nat Methods, 2017. **14**(7): p. 645-646.

89. Szklarczyk, D., et al., *STRING v11: protein-protein association networks with increased coverage, supporting functional discovery in genome-wide experimental datasets.* Nucleic Acids Res, 2019. **47**(D1): p. D607-d613.

90. James, C., et al., *Proteomic mapping by rapamycin-dependent targeting of APEX2 identifies binding partners of VAPB at the inner nuclear membrane.* J Biol Chem, 2019. **294**(44): p. 16241-16254.

91. Wu, R., et al., *Hsp27 regulates Akt activation and polymorphonuclear leukocyte apoptosis by scaffolding MK2 to Akt signal complex.* Journal of Biological Chemistry, 2007. **282**(30): p. 21598-21608.

92. Jaco, I., et al., *MK2 phosphorylates RIPK1 to prevent TNF-induced cell death.* Molecular cell, 2017. **66**(5): p. 698-710. e5.

93. Neininger, A., et al., *MK2 targets AU-rich elements and regulates biosynthesis of tumor necrosis factor and interleukin-6 independently at different post-transcriptional levels.* Journal of Biological Chemistry, 2002. **277**(5): p. 3065-3068.

94. Zu, Y.-L., et al., *The primary structure of a human MAP kinase activated protein kinase 2.* Biochemical and biophysical research communications, 1994. **200**(2): p. 1118-1124.

95. Chen, I.T., et al., *Promyelocytic leukemia protein targets MK2 to promote cytotoxicity.* EMBO reports, 2021. **22**(12): p. e52254.

96. White, A., et al., *Molecular basis of MAPK-activated protein kinase 2: p38 assembly.* Proceedings of the National Academy of Sciences, 2007. **104**(15): p. 6353-6358.

97. Oughtred, R., et al., *The BioGRID interaction database: 2019 update.* Nucleic acids research, 2019. **47**(D1): p. D529-D541.

98. Alsheich-Bartok, O., et al., *PML enhances the regulation of p53 by CK1 in response to DNA damage.* Oncogene, 2008. **27**(26): p. 3653-3661.

99. Yu, J., et al., *PML3 interacts with TRF1 and is essential for ALT-associated PML bodies assembly in U2OS cells.* Cancer letters, 2010. **291**(2): p. 177-186.

100. Dellaire, G., et al., *Mitotic accumulations of PML protein contribute to the re-establishment of PML nuclear bodies in G1.* Journal of cell science, 2006. **119**(6): p. 1034-1042.

101. Shav-Tal, Y., et al., *Dynamic sorting of nuclear components into distinct nucleolar caps during transcriptional inhibition.* Molecular biology of the cell, 2005. **16**(5): p. 2395-2413.

102. Corpet, A., et al., *PML nuclear bodies and chromatin dynamics: catch me if you can!* Nucleic Acids Research, 2020. **48**(21): p. 11890-11912.

103. Pinder, J., J. Salsman, and G. Dellaire, *Nuclear domain 'knock-in'screen for the evaluation and identification of small molecule enhancers of CRISPR-based genome editing.* Nucleic acids research, 2015. **43**(19): p. 9379-9392.

104. Katzmann, D.J., M. Babst, and S.D. Emr, *Ubiquitin-dependent sorting into the multivesicular body pathway requires the function of a conserved endosomal protein sorting complex, ESCRT-I.* Cell, 2001. **106**(2): p. 145-155.

105. Futter, C.E., et al., *Multivesicular endosomes containing internalized EGF-EGF receptor complexes mature and then fuse directly with lysosomes.* The Journal of cell biology, 1996. **132**(6): p. 1011-1023.

106. Wang, J., et al., *An ESCRT-dependent step in fatty acid transfer from lipid droplets to mitochondria through VPS13D− TSG101 interactions.* Nature communications, 2021. **12**(1): p. 1-16.

107. Lin, Y.-S., et al., *Identification of TSG101 functional domains and p21 loci required for TSG101-mediated p21 gene regulation.* PLoS One, 2013. **8**(11): p. e79674.

108. Jensen, D. and R. Schekman, *COPII-mediated vesicle formation at a glance.* Journal of cell science, 2011. **124**(1): p. 1-4.

109. Klumperman, J., et al., *The recycling pathway of protein ERGIC-53 and dynamics of the ER-Golgi intermediate compartment.* Journal of cell science, 1998. **111**(22): p. 3411-3425.

110. Yehia, L., et al., *Non-canonical role of wild-type SEC23B in the cellular stress response pathway.* Cell death & disease, 2021. **12**(4): p. 1-12.

111. Condemine, W., et al., *A nucleolar targeting signal in PML-I addresses PML to nucleolar caps in stressed or senescent cells.* Journal of cell science, 2007. **120**(18): p. 3219-3227.

112. Nguyen, L.A., et al., *Physical and functional link of the leukemia-associated factors AML1 and PML.* Blood, 2005. **105**(1): p. 292-300.

113. Hsu, K.-S. and H.-Y. Kao, *PML: Regulation and multifaceted function beyond tumor suppression.* Cell & bioscience, 2018. **8**(1): p. 1-21.

114. Timney, B.L., et al., *Simple rules for passive diffusion through the nuclear pore complex.* Journal of Cell Biology, 2016. **215**(1): p. 57-76.

115. Rickard, J.A., et al., *RIPK1 regulates RIPK3-MLKL-driven systemic inflammation and emergency hematopoiesis.* Cell, 2014. **157**(5): p. 1175-1188.

116. Fukuyo, Y., et al., *Phosphorylation-Dependent Lys63-Linked Polyubiquitination of Daxx Is Essential for Sustained TNF-α–Induced ASK1 Activation.* Cancer research, 2009. **69**(19): p. 7512-7517.

117. Charette, S.J., et al., *Inhibition of Daxx-mediated apoptosis by heat shock protein 27.* Molecular and cellular biology, 2000. **20**(20): p. 7602-7612.

118. Platanias, L.C., *The p38 mitogen-activated protein kinase pathway and its role in interferon signaling.* Pharmacology & therapeutics, 2003. **98**(2): p. 129-142.

119. Uddin, S., et al., *The Rac1/p38 mitogen-activated protein kinase pathway is required for interferon α-dependent transcriptional activation but not serine phosphorylation of Stat proteins.* Journal of Biological Chemistry, 2000. **275**(36): p. 27634-27640.